nature reviews earth & environment

https://doi.org/10.1038/s43017-025-00746-y

Review article

Check for updates

Southern Annular Mode dynamics, projections and impacts in a changing climate

Ariaan Purich[1,2] ✉, Julie M. Arblaster[1,2,3], Ghyslaine Boschat[3,4], Zoe E. Gillett[3,4], Will Hobbs[5,6], Martin Jucker[7], Eun-Pa Lim[4], Danielle Udy[4,5,6,8], Nerilie Abram[8,9], Elio Campitelli[1,2], Edward Doddridge[5,6], Matthew H. England[10], Andrew King[3,11], Laurie Menviel[7,8], Amelie Meyer[3,5,6,8], Valentina Ortiz Guzmán[3,7], Raina Roy[1,2], Irina Rudeva[4], Paul Spence[5,8,12], Peter G. Strutton[3,5,8] & Tilo Ziehn[13]

Abstract

The Southern Annular Mode (SAM) influences Southern Hemisphere temperature and precipitation, ocean circulation, carbon cycling and the Antarctic cryosphere. In this Review, we examine the dynamics, projections and effects of the SAM, focusing on future implications for the Southern Ocean and Antarctica. The SAM is the leading mode of atmospheric variability in the Southern Hemisphere extratropics, associated with variations in the mid-latitude westerly jet strength and position. The SAM is primarily an internally driven atmospheric process, for which anomalies dissipate in 1–2 weeks; however, sustained SAM anomalies can also be forced by stratospheric processes and tropical Pacific variability. Ozone depletion during the 1970s–1990s contributed to large positive trends in austral summer. The SAM is now in its most positive mean state in over 1,000 years, and a year-round positive trend in the SAM is projected to continue throughout the twenty-first century in response to increasing greenhouse gases. Given the importance of SAM effects on Southern Ocean circulation, carbon cycling, and Antarctic ice mass balance for future climate and sea level rise projections, it is crucial that the effects of SAM are better modelled and understood, including accounting for the influence of the shifting seasonality of positive SAM trends and its increasing asymmetry.

Sections

A full list of affiliations appears at the end of the paper. ✉e-mail: ariaan.purich@monash.edu

Introduction

The Southern Annular Mode (SAM) is the leading mode of extratropical Southern Hemisphere weather and climate variability, describing fluctuations in pressure between the high and mid latitudes, and in the position and strength of the mid-latitude westerly jet on daily, monthly and decadal timescales[1,2] (Fig. 1a). Positive SAM is defined as concurrent lower-than-normal pressure over the Antarctic region and higher-than-normal pressure in the mid latitudes, which occurs predominantly with a poleward shift of the tropospheric mid-latitude jet (Fig. 1a,b) and explains 50–70% of the monthly zonal-mean zonal wind variability (Fig. 1c, yellow line). Negative SAM involves opposite pressure changes, with an equatorward shift of the mid-latitude jet. The effects of the SAM extend across the Southern Hemisphere, connecting processes from the stratosphere, through the troposphere to the ocean, and from Antarctica to the tropics (Fig. 1a,b).

There are various definitions of the SAM index. These definitions are based on the difference between the standardized mean sea level pressure (MSLP) at 40° S and 65° S (ref. 3) (Fig. 1c, black line), the difference between standardized MSLP observations from mid-latitude (37–47° S) and Antarctic (65–71° S) stations[4] (Fig. 1c, blue line), and empirical orthogonal function analysis of extratropical Southern Hemisphere tropospheric fields such as MSLP, geopotential height and zonal wind[1,5] (Fig. 1c, red line). SAM indices calculated with these definitions are highly correlated[6] (Fig. 1c). However, standardization at different temporal resolutions can introduce discrepancies in the amplitude of annual SAM index variations[7,8], with annual normalization yielding a higher amplitude than calculating an annual SAM index from monthly data[8]. In this Review, the SAM index is calculated using the MSLP difference definition[3], using monthly data over 1979–2023, with seasonal or annual averages then constructed as required.

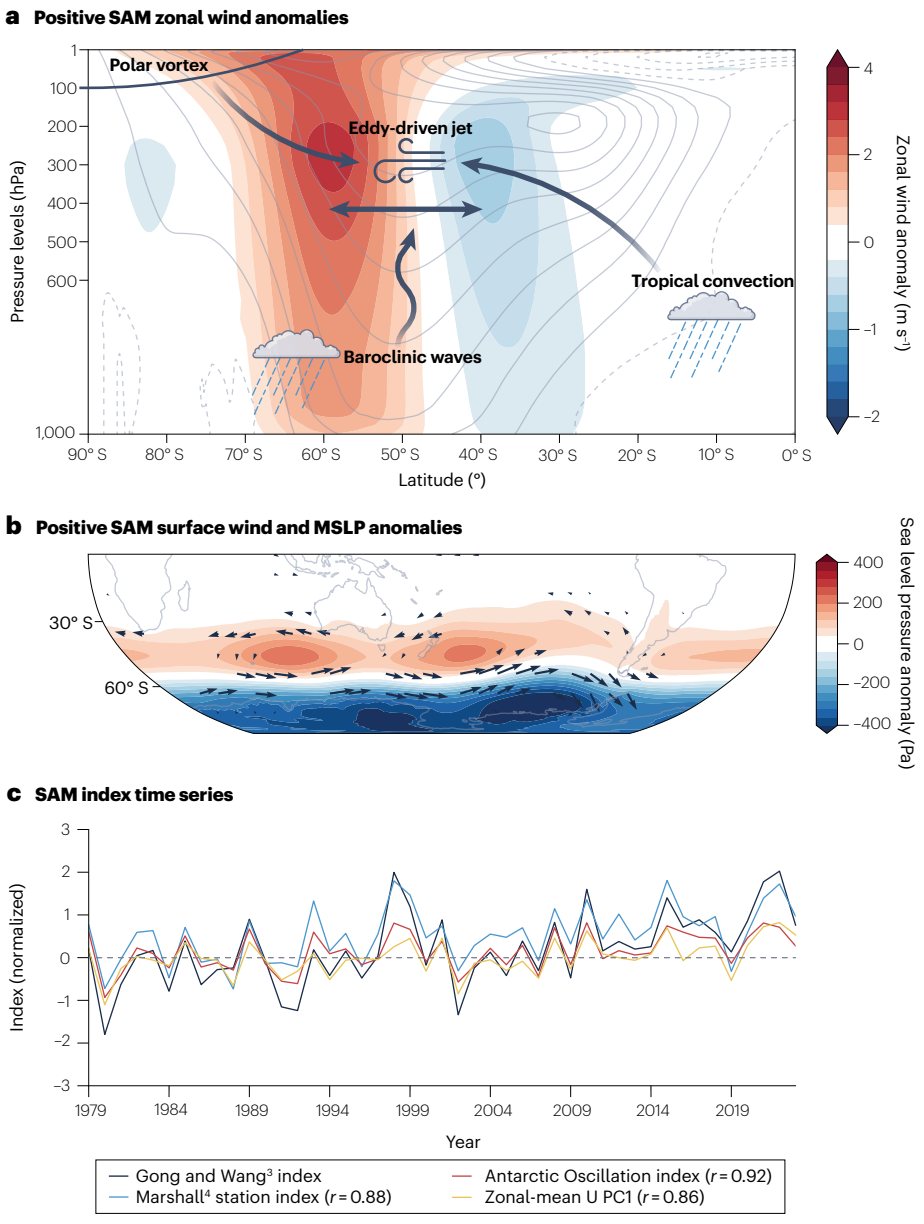

Fig. 1 | Zonal-mean and surface anomalies associated with positive SAM and time series. **a**, The monthly zonal-mean zonal wind[201] anomalies regressed onto the monthly standardized Southern Annular Mode (SAM) index over 1979–2023 (shading), the climatological zonal-mean zonal wind (grey contours) and key influences on the position and intensity of the mid-latitude jet (schematic additions). The solid and dashed contours represent westerly and easterly climatological winds, respectively. **b**, The monthly surface wind anomalies[201] (vectors) and mean sea level pressure[201] (MSLP) anomalies (shading) regressed onto the monthly standardized SAM index over 1979–2023. **c**, Different representations of the SAM index time series over 1979–2023 based on the difference between the standardized zonal-mean MSLP at 40° S and the standardized zonal-mean MSLP at 65° S (Gong and Wang index[3]), the difference in surface pressure based on observations from six stations ~40° S and six stations ~65° S (Marshall station index[4]), the projection of the 700-hPa geopotential height anomalies onto the Antarctic Oscillation loading pattern[1] (Antarctic Oscillation index) and the first principal component (PC1) of zonal-mean zonal wind[16] (U) that captures the meridional shift of the mid-latitude jet (zonal-mean U PC1). Correlation coefficients (*r*) between the Gong and Wang index and the other indices are included in the legend. In panels **a** and **b**, the SAM is calculated using the Gong and Wang definition[3]. In all panels, the SAM is calculated for each month before annual averaging. Anomalies are calculated relative to the 1981–2010 baseline. The SAM exhibits a clear positive trend over the satellite era, with atmospheric anomalies of positive SAM connecting processes from the stratosphere through the troposphere, and from Antarctica to the tropics.

Variations in the SAM influence surface weather and climate across the Southern Hemisphere. In late austral spring 2019, a record-negative SAM for the season contributed to unusually persistent hot and dry conditions across subtropical eastern Australia[9], exacerbating extreme wildfires[10,11]. Additionally, surface wind changes drive Southern Ocean circulation, which can affect the uptake and transport of heat and carbon in the ocean. SAM affects Antarctic mass changes through two mechanisms: atmospherically driven changes in precipitation accumulation influence the surface mass balance[12], and wind-driven ocean heat transport onto the continental shelf influences the basal melting of ice shelves that buttress ice sheets. This Review focuses on the SAM effect over the Southern Ocean and Antarctica; the mid-latitude effects have been reviewed previously[13].

Since the mid-twentieth century, the SAM has trended towards its positive phase[4,13]. Projections under high and very high greenhouse gas emission scenarios suggest that this positive trend will continue throughout the twenty-first century, although the seasonality of trends in the SAM is expected to change[14]. It is important to understand how the SAM will change to inform projections of Southern Hemisphere surface climate, the Southern Ocean and Antarctic cryosphere over the twenty-first century and beyond.

This Review explores how variations in the SAM, through variations in the mid-latitude westerly jet, affect the Southern Hemisphere climate. First, we describe the dynamics and drivers of SAM variability across seasons. Next, we discuss the observed trends and variability of the SAM over the instrumental record and palaeoclimate reconstructions of the past millennium, and examine future projections of the SAM. We consider the effects of the SAM on Southern Hemisphere climate, with a focus on Southern Ocean circulation and the carbon cycle, and on the Antarctic cryosphere. Finally, we outline limitations of the current understanding of the SAM and further work that is needed to address them.

Dynamics and drivers of SAM

To understand the observed and projected changes in the SAM and its effects on Southern Hemisphere climate, this Review begins by exploring the physical processes that promote SAM variability. The dynamical foundations of the SAM are described, starting with the structure and seasonal cycle of the Southern Hemisphere extratropical jets. Both zonal-mean dynamics and zonal asymmetries in the SAM structure and mechanisms are considered, as well as interactions with other climate modes and their role in seasonal predictability of the SAM.

Southern Hemisphere tropospheric jets

The Southern Hemisphere extratropical tropospheric circulation is dominated by two strong westerly jets, the subtropical jet and the mid-latitude eddy-driven jet (ref. 5) (Fig. 1a), each exhibiting distinct structural and seasonal characteristics. The subtropical jet forms near 200 hPa and 30° S through differential heating between the tropics and subtropics. This jet is strongest in austral winter (June–August) and weakest in summer (December–February), when it merges with the eddy-driven jet (Fig. 2). The vertical structure of the subtropical jet is strongly baroclinic, with easterlies at the surface and westerlies aloft[15] (for the annual mean, see Fig. 1a). In contrast, the eddy-driven jet has an equivalent barotropic vertical structure. This jet forms at around 50° S (Figs. 1a and 2a–d) and is driven by baroclinic eddies forced by the strong year-round meridional gradient in Southern Ocean sea surface temperature[16].

Zonal-mean dynamics

The primary intrinsic mechanism for the persistence of the SAM is the positive feedback between the extratropical zonal wind and baroclinic eddies. During positive SAM, westerly anomalies in the mid-to-upper troposphere on the poleward side of the climatological mid-latitude westerly jet coincide spatially with regions of anomalous eddy momentum flux convergence, whereas easterly anomalies on the equatorward side coincide with anomalous eddy momentum flux divergence[1,16,17]. The positive feedback between the eddy momentum flux convergence anomalies and the jet anomalies thus maintains the poleward-shifted jet against surface friction and reinforces the positive SAM anomaly.

Zonal asymmetries

Although the SAM is characterized by an annular structure, there are distinct regional and seasonal differences in its dynamics and structure (Fig. 2). These seasonal differences and regional behaviours are linked to the structure of the mid-latitude westerly jet[18–20] (Fig. 2a–d, climatological contours). From late spring to summer, the mid-latitude jet becomes more zonally symmetric, promoting a positive zonally symmetric eddy feedback across most longitudes that drives a meridional shift of the jet. As a result, the SAM in summer describes a north–south shift of the mid-latitude westerly jet about its climatological latitude[18–20] (poleward for positive SAM and equatorward for negative SAM; Fig. 2a,c,e). In contrast, during winter to early spring, the mid-latitude jet is strongest over the Indian Ocean, where a positive eddy feedback supports meridional shifts of the jet (Fig. 2b,d,f). Over the western Pacific, the subtropical jet dominates and acts as a strong zonal waveguide, trapping Rossby waves[21,22]. In this region, there is no eddy feedback, and meridional shifts of the mid-latitude jet are restricted. Therefore, in winter to early spring, the SAM reflects in-place variations in the strength of the jets in this western Pacific sector[18–20] (Fig. 2f).

The surface expression of the SAM in the pressure field exhibits seasonally varying zonal asymmetry. This asymmetric nature can be described by differencing the western and eastern hemispheres[20,23] or examining deviations of the SAM from the zonal mean[24,25] (Fig. 3). Deviations from the zonal mean account for up to 20% of total SAM variability (Fig. 3d), depending on the time period, time of year and averaging period[24]. This asymmetry is most pronounced outside of summer (Fig. 3d) in regions south of 50° S (refs. 24,26,27) (Fig. 3c) and during negative SAM phases (Fig. 2d), which have stronger zonally asymmetric features than positive phases[24]. The asymmetry is characterized mainly by planetary wave activity, particularly wavenumbers 1 and 3, with maximum amplitude in the South Pacific[25,27,28], resembling the Pacific–South American pattern[20,24,25,29], and teleconnecting to the Amundsen Sea Low[30,31] (Fig. 3a). There is some evidence for a positive trend in the strength of the zonally asymmetric component of the SAM over the satellite era[32], despite the positive summer trend being evident only in the symmetric SAM component[24,25,32].

Interactions between SAM and other climate modes

The Antarctic stratospheric vortex and associated ozone variations are the largest driver of SAM variability (Figs. 1a and 3e, light-blue line). The variability of the Antarctic stratospheric polar vortex peaks in austral spring. Throughout spring and summer, stratospheric temperature and zonal wind anomalies move downwards towards the troposphere via active feedback between waves and mean flow[33–37]. The downward propagation of these stratospheric vortex anomalies leads

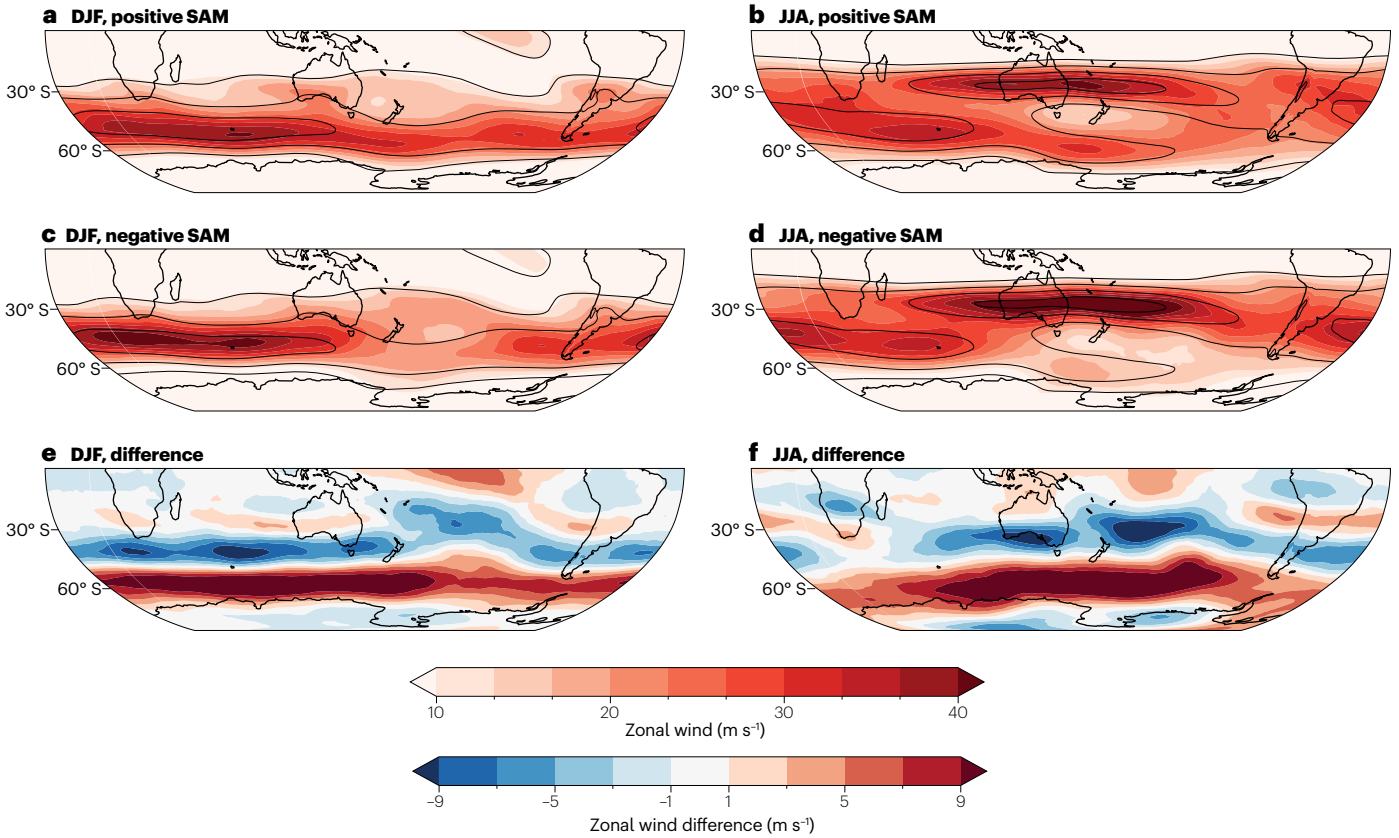

Fig. 2 | Seasonal 300-hPa zonal wind for positive and negative SAM, and the differences. a, A composite of austral summer (December–February; DJF) 300-hPa zonal wind[201] when the Southern Annular Mode (SAM) index is ≥2 (positive SAM) over 1979–2023. The black contours reflect the climatological zonal wind, drawn at 10, 20, 30 and 40 m s^{-1}. **b**, As in panel **a**, but for events where the SAM index is ≤−2 (negative SAM). **c**, The difference between positive and negative SAM events in DJF (that is, panel **a** minus **b**). **d**–**f**, As in panels **a**–**c**, but for austral winter (June, July, August; JJA). The single westerly jet at ~50° S is evident in summer (DJF) for both positive and negative SAM, but during winter (JJA) the split jet structure is evident, with the subtropical jet over Australia.

to a persistently anomalous SAM state; however, the detailed mechanism remains unclear. A modulation of the polar tropopause height by the stratospheric temperature and circulation anomalies is key to promoting an annular mode response by redistributing tropospheric mass over the polar region[38,39]. Furthermore, a two-way positive feedback between the Antarctic stratospheric polar vortex and Antarctic lower stratosphere ozone concentration amplifies anomalies over the polar cap region[40], with polar vortex variability explaining 25–50% of SAM variance in austral warm seasons (Fig. 3e). For instance, a strong vortex is associated with low temperatures, which increases polar stratospheric clouds. The increased cloud facilitates ozone depletion, which lowers the polar cap temperature and strengthens the vortex. These anomalies gradually move down to the troposphere as the season progresses and the mean vortex winds become weaker, steepening the tropospheric meridional temperature gradient and driving a poleward shift of the mid-latitude eddy-driven jet, which is depicted as a positive phase of the SAM[40,41].

The El Niño Southern Oscillation (ENSO) is a secondary driver of SAM variability, explaining up to 10% of SAM variance (Fig. 3e, red line). ENSO influences the symmetric components of SAM by changing the latitudinal extent of the downwards branch of the Hadley circulation, and the asymmetric components of SAM via the Pacific–South American pattern[29,42]. For the symmetric component, cooling in the tropics during La Niña weakens and expands the Hadley circulation, shifting the subtropical jet and associated critical latitude poleward[43,44]. Consequently, anomalous eddy momentum flux divergence increases in the mid latitudes, inducing anomalous poleward and downward motions and associated adiabatic warming in higher latitudes[17]. The resultant sharpening of the meridional temperature gradient promotes eddy generation, and the subsequent eddy–mean-flow feedback results in persistent positive SAM[43–45]. This zonally symmetric ENSO–SAM interaction is most prominent from spring to summer, when ENSO has a large amplitude and the subtropical jet is relatively weak (Fig. 3e). For the asymmetric component, in winter, the central Pacific ENSO (El Niño Modoki) contributes to SAM variability (Fig. 3e, yellow line) by modulating the Pacific–South American pattern[19,20] and meridionally shifting the subtropical jet[46,47].

Dynamical links to climate modes allows the seasonal prediction of the SAM. The established relationship between the SAM and the Antarctic polar vortex and ENSO enables the seasonal prediction of the SAM from austral early spring to early summer (Fig. 3e, dark-blue line). A dynamical seasonal forecast system[48] initialized with high-quality observational data skilfully predicts the seasonal SAM almost year

round at the shortest lead time (Fig. 3e, dashed black line). This system demonstrates the highest skill in spring to early summer, with lead times of up to a season, which is consistent with the predictability achieved using the relationship of the SAM with the stratospheric polar vortex and ENSO[48].

On decadal timescales, variability in the tropical Pacific can influence the SAM in a manner similar to ENSO[49]. The cold phase of the Interdecadal Pacific Oscillation sets a sharp meridional temperature gradient between 40° S and 60° S. Simulations with a coupled climate model suggest that this cold phase of the Interdecadal Pacific Oscillation can cause high-speed eddies to travel faster (similar to the global warming-driven mechanism[43]) and low-speed eddies to break at higher latitudes (similar to the La Niña-driven mechanism). Consequently, the Interdecadal Pacific Oscillation forced a weak positive SAM trend in the early twenty-first century[50], despite a slight reversal of ozone depletion during the 2000s–2010s (ref. 51).

Other modes of climate variability do not appear to have a strong influence on the SAM. Although a relationship between convection related to the Madden–Julian Oscillation and the SAM is sometimes identified, there is generally a lack of phase coherence between them[52–55]. Furthermore, anomalies related to the Madden–Julian Oscillation in the higher southern latitudes also lack an annular nature. The relationship between the Indian Ocean Dipole and SAM was significant in austral spring for the 1980–1990s (ref. 56), but it is only moderate over 1979–2023 (not shown), and the mechanism behind the interaction is unclear.

Trends and projections of SAM

Understanding the characteristics of the SAM provides context for understanding its changes on interannual to centennial timescales. This section highlights the observed and projected trends in the SAM and our understanding of their causes. It examines reconstructions over

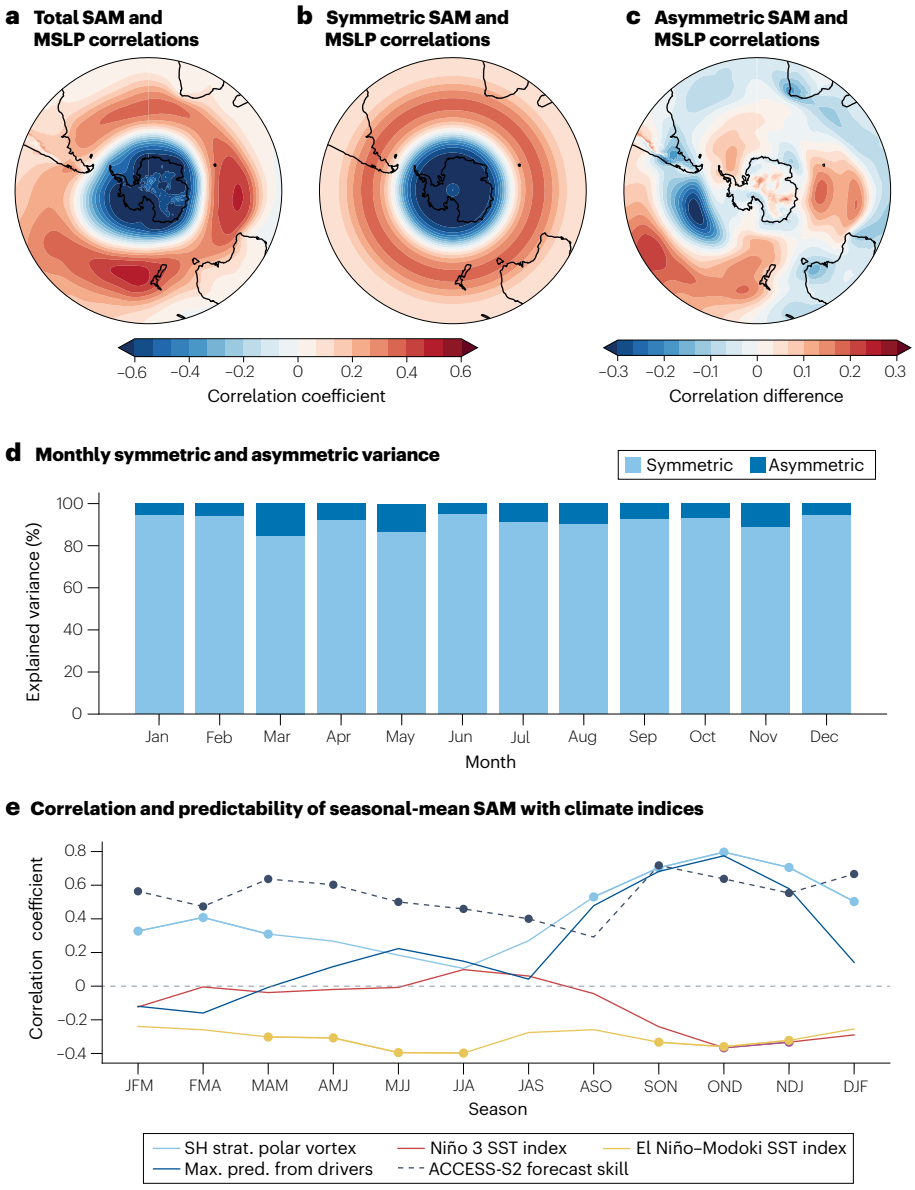

Fig. 3 | Symmetric and asymmetric components of the SAM and relationships with drivers. **a**, The correlations between monthly mean sea level pressure[201] (MSLP) and the total Southern Annular Mode (SAM) index over 1979–2023. **b**, As in panel **a**, but for the correlations between MSLP and the symmetric component of the SAM, calculated as the zonal mean of the full field. **c**, As in panel **a**, but for the correlations between MSLP and the asymmetric component of the SAM, calculated as the difference between the total field and the zonal mean (that is, panel **a** minus panel **b**). **d**, The monthly variance explained by the symmetric (light blue) and asymmetric (dark blue) components of the SAM. **e**, Running correlations between the SAM index and its drivers (Southern Hemisphere stratospheric (SH strat.) polar vortex[202] (light blue), Niño 3 sea surface temperature (SST) index[203] (red) and El Niño–Modoki SST index[204] (yellow)) over 1979–2022, the maximum prediction (max. pred.) skill offered by the three drivers combined (dark blue) and the forecast skill for ACCESS-S2 (ref. 48) simulations initialized on the first day of each season (dashed black) over 1982–2018. The dots indicate statistical significance at $P < 0.05$. Although the SAM is characterized by an annular structure, it also exhibits an asymmetric component that varies seasonally and is linked with tropical variability.

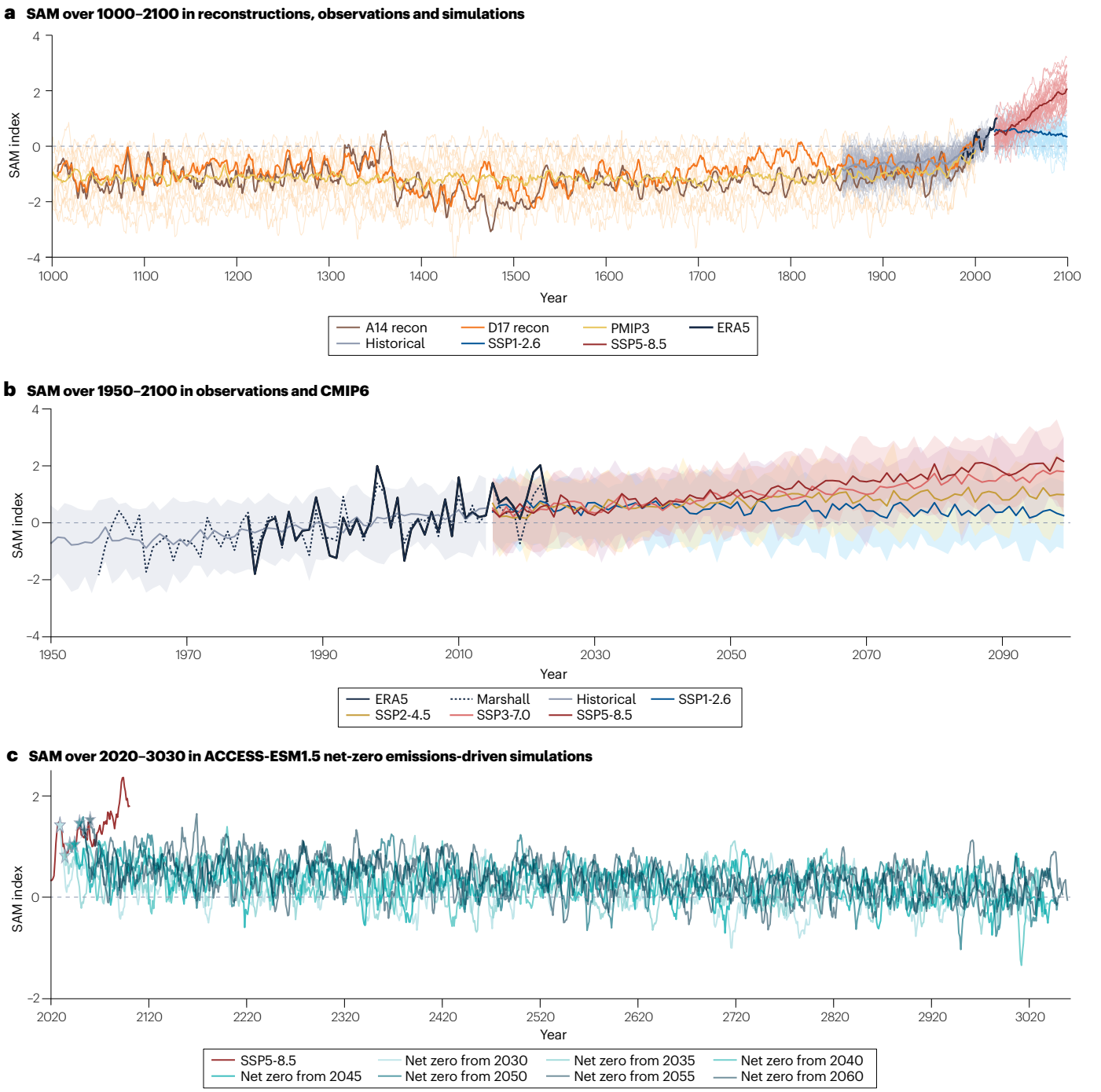

Fig. 4 | Past, present and future evolution of the SAM. a, The 7-year running mean annually averaged Southern Annular Mode (SAM) index across palaeoclimate reconstructions (recon) (A14 (ref. 57) and D17 (ref. 58)); Paleoclimate Modelling Intercomparison Project phase 3 (PMIP3) simulations[199] over 1000–2000; Coupled Model Intercomparison Project phase 6 (CMIP6) historical and future simulations[198] over 1850–2100, with the future projections encompassing a low (Shared Socioeconomic Pathway (SSP)1-2.6) and very high (SSP5-8.5) emissions scenario; and ERA5 reanalysis[201] over 1979–2023. For PMIP3 and CMIP6 data, the thin lines represent individual models, and bold lines represent the multimodel mean. **b**, The annually averaged SAM index from CMIP6 historical simulations over 1950–2014; CMIP future simulations under SSP1-2.6, SSP2-4.5, SSP3-7.0 and SSP5-8.5 over 2015–2100; ERA5 over 1979–2023; and the Marshall index[4] based on station pressure observations over 1957–2023. The shading represents the 5–95th percentile range across models and bold lines show the multimodel mean. **c**, Millennial evolution of the 7-year running mean SAM in ACCESS-ESM1.5 (ref. 76) from net-zero emissions-driven simulations, branched 5-yearly from 2030 to 2060 from SSP5-8.5 (branch points indicated by stars) and run for 1,000 years. In all panels, the SAM is calculated using the Gong and Wang definition[3], using monthly mean sea level pressure before annual averaging. Anomalies are calculated relative to the 1981–2010 baseline. Observational evidence indicates that the SAM has trended towards the positive phase since the mid-twentieth century, outside the range seen over the last millennium, and that this trend is projected to continue into the future unless net-zero emissions are achieved.

the past 1,000 years (Fig. 4a), observations and reanalyses over more recent decades (Fig. 4b), and our mechanistic understanding through simulations with various external forcings (Fig. 4).

Past SAM evolution

Reconstructions of the annual[57,58] and summer[58,59] SAM indices have been developed using various combinations of palaeoclimate proxies (Fig. 4a). These reconstructions combine Southern Hemisphere proxies and are assessed using direct correlation to observational SAM indices. A proxy–model assimilation framework has also been used to reconstruct the summer SAM, with the post-1400 CE part of this reconstruction relying on secondary tree-ring-derived gridded drought atlas reconstructions alongside the primary proxy network[60]. Reconstructions are generally more reliable for summer SAM reconstructions than for annual-mean reconstructions[58]. Some of these reconstructions disagree on the scale of the SAM index variability[58,60]. This mismatch is attributed to scaling differences in the instrumental target data used for each reconstruction[7] and can be reconciled by using a consistent methodology to calculate the SAM index[7,8].

SAM reconstructions often feature large pre-industrial SAM variability. This natural variability includes an abrupt, century-scale negative trend around the 1400s, followed by a multicentury trend towards more positive SAM between ~1500 and 1800 CE[57–59] in all but the data-assimilation version of the reconstructed SAM[57–59] (Fig. 4a, brown and orange lines). Similar trends spanning multiple centuries are not observed in individual model simulations of the past millennium[57] (Fig. 4a, PMIP3 simulations). This apparent stability of the modelled SAM could be caused by incomplete representation of solar forcing[7]. Nevertheless, the pre-industrial variability and trends in SAM reconstructions lie within the range of natural variability of past millennium simulations[58,60] (Fig. 4a), and there is no evidence to connect pre-industrial summer SAM variability to solar, volcanic or greenhouse gas forcings[58,60].

Over the satellite era (1979–2023), the SAM has trended towards a more positive phase[4,13,61] (Fig. 4a), particularly in austral summer. The mean summer and annual SAM is now in its most positive mean state in more than 1,000 years (refs. 57,59) (Fig. 4a). This trend in the summer SAM falls outside the two standard deviation range of pre-industrial trends during the Common Era[58,60].

Attribution of SAM trends

SAM trends over the satellite era are reproduced by historical experiments of Coupled Model Intercomparison Project phase 6 (CMIP6) models driven by anthropogenic and natural forcings (Fig. 4b). The SAM responds strongly to this external forcing; however, the sensitivity to different forcings is uncertain and model dependent (Fig. 5). Among these forcings, Antarctic ozone depletion has a key role, predominantly cooling the polar stratosphere in austral spring when the ozone hole first forms. This stratospheric cooling strengthens the stratospheric winds and delays the breakdown of the stratospheric polar vortex. These changes lead to a poleward shift in the tropospheric mid-latitude jet and a positive SAM trend in summer[51,62] (Fig. 5a,b). Models forced with ozone depletion (such as in the hist-stratO3 experiment) can broadly capture these changes[51,63–66], with a positive SAM trend in summer, but the exact mechanism through which the stratospheric signature of ozone depletion affects the troposphere and surface response is not fully understood[67].

The SAM is also sensitive to changing concentrations of greenhouse gases, but through different mechanisms. Increasing greenhouse gas concentrations warm the tropical upper troposphere and cool the polar stratosphere, steepening the meridional temperature gradient in the Southern Hemisphere. Consequently, thermal wind balance leads to a strengthening of the subtropical jet[67]. This response of the mid-latitude westerly jet and the resulting positive SAM trend are thought to be linked to diabatic processes in the subtropics and mid latitudes that modulate the structure of the Ferrel cell (refs. 68,69) or increase the moisture gradient[70]. However, the jet shift could also be attributed to eddy–mean-flow feedback arising from an increase in the eddy phase speeds, which causes them to break on the equatorward side of the mid-latitude jet before reaching the subtropical jet[43,67]. Models forced with greenhouse gases (such as in the greenhouse gas forcing only (hist-GHG) experiment) simulate a positive SAM trend in both summer (Fig. 5a,b) and winter[63] (Fig. 5c,d).

Ozone depletion and greenhouse gases have both had identifiable influences on observed historical SAM trends. Greenhouse gases monotonically increased over the historical period and continue to increase. Conversely, Antarctic stratospheric ozone was substantially depleted (by up to ~50% in spring[51]) from the 1970s to the 1990s and began to recover (or at least stabilize) from ~2000 onwards, with a full recovery expected by the 2060s (ref. 51). Larger positive SAM trends are found in summer than winter during 1979–1999, when the influence of ozone depletion and greenhouse gas increases combine[13] (Fig. 5a,c). Long-term SAM reconstructions suggest that the current positive SAM trends began around the 1940s[57] (Fig. 4a), which is too early to be attributed to ozone forcing alone. However, this early onset is consistent with simulations that include greenhouse gas forcing without the additional influence of ozone depletion[57]. Thus, although the positive summer trend is primarily attributed to ozone depletion[51,63–66], increased greenhouse gas concentrations also contribute[63] (Fig. 5).

Weakening positive SAM trends are found over the ozone stabilization period (2000–2014) in austral summer (Fig. 5a). Both reanalysis and the historical experiments have weaker summer SAM trends for the ozone stabilization period (0.61 and 0.09 per decade, respectively, for ERA5 and the historical multimodel median; Fig. 5a, 2000–2014) than for the ozone depletion period (1.50 and 0.54 per decade, respectively; Fig. 5a, 1979–1999). Additionally, ozone forcing only (hist-stratO3) experiments exhibit negative trends (−0.43 per decade for the multimodel median; Fig. 5a, 2000–2014). This weakening of summer SAM trends might indicate the beginning of a reversal in the SAM trends[51,71] associated with ozone recovery[51,67,72]; however, there is sensitivity to the choice of start and end points in trends calculated over short time series[67].

There is large variation between experiments in the modelled response of the SAM to individual forcings. CMIP6 hist-stratO3 simulations exhibit more positive summer SAM trends (0.21 per decade for the multimodel median) than hist-GHG simulations (0.13 per decade) over the ozone depletion period (Fig. 5a, 1979–1999). The specific ozone forcing magnitude also influences the response of the SAM to ozone depletion. For example, one hist-stratO3 simulation, which uses weak ozone forcing, exhibits a negative SAM trend[63] (Fig. 5a). There is also large variation across the ensemble means of the individual models (Fig. 5a,c, large grey dots) and individual members (Fig. 5a, box and whiskers) in both seasons and periods of the hist-GHG and hist-stratO3 experiments, with the interquartile range spanning zero. Some of this variation might stem from internally generated variability from the tropical Pacific (discussed above), which contributes to observed multidecadal changes in the SAM and mid-latitude jet[50,73,74].

Projections of the SAM

Future SAM trends are projected to remain positive under high-emission scenarios. CMIP6 projections under high and very high greenhouse gas

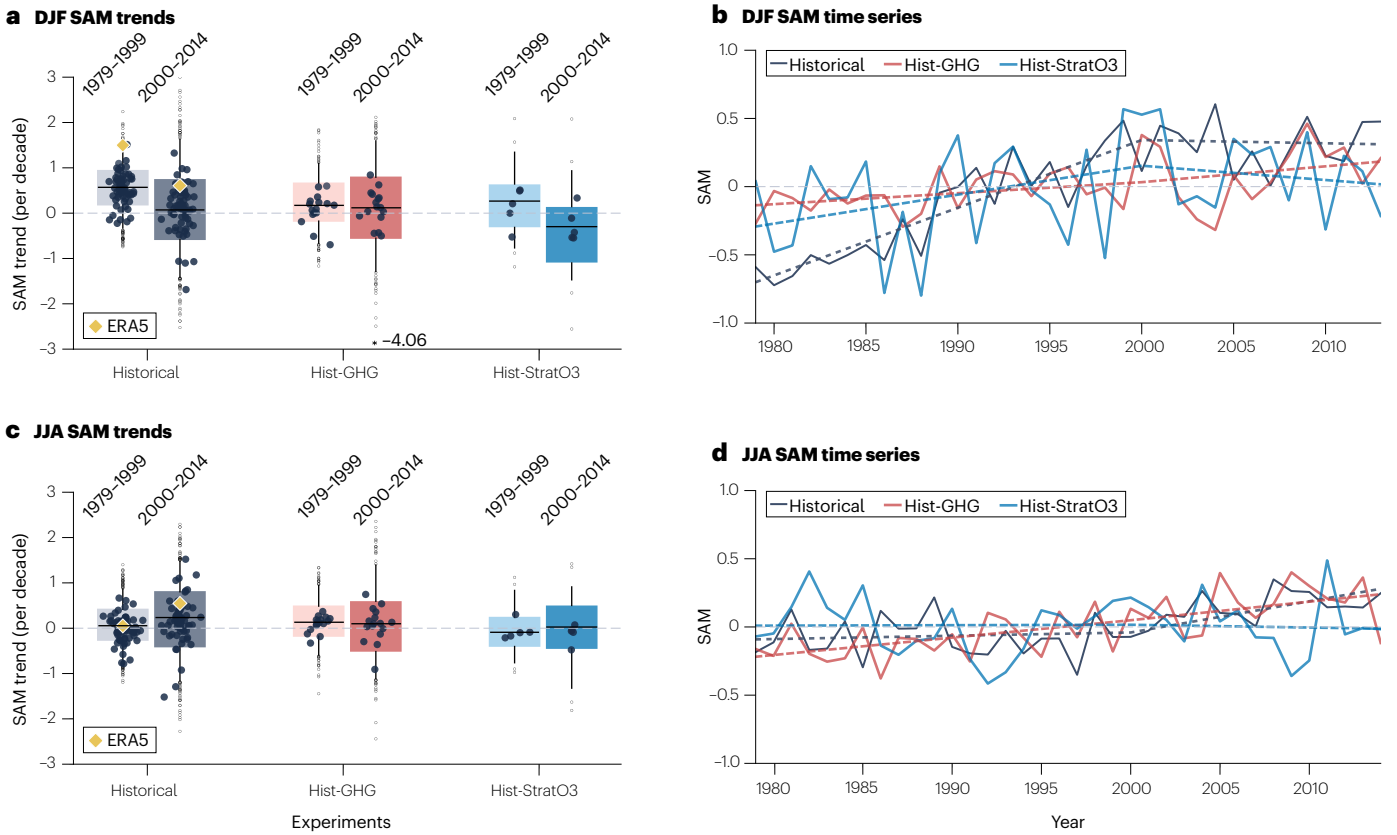

Fig. 5 | Historical SAM trend attribution. a, Austral summer (December, January, February; DJF) Southern Annular Mode (SAM) trends in Coupled Model Intercomparison Project phase 6 simulations[198] with all historical forcings (historical), greenhouse gas forcing only (hist-GHG) and ozone forcing only (hist-stratO3). Trends are calculated over 1979–1999 (ozone depletion period) and 2000–2014 (ozone stabilization period) for all individual simulations, with box plots indicating the ensemble median (solid bar), interquartile range (box), 5–95th percentiles (whiskers) and outliers (small dots). The large dots represent the ensemble mean of each model, and the yellow diamonds show the ERA5 trends. **b**, Multimodel mean summer (DJF) SAM index time series for the historical (grey), hist-GHG (red) and hist-stratO3 (blue) experiments, overlaid with piece-wise linear trends (dashed lines) for the ozone depletion (1979–1999) and stabilization (2000–2014) periods. **c**,**d**, As in panels **a** and **b** but for austral winter (June, July, August; JJA). The SAM has been influenced by ozone depletion from the 1970s to the 1990s, with the onset of ozone recovery evident in the stabilization of summer (DJF) SAM trends from ~2000 onwards. The influence of increasing greenhouse gas concentrations is evident in the positive trend in the winter (JJA) SAM.

emission Shared Socioeconomic Pathway (SSP) scenarios suggest that positive trends in annual SAM will continue throughout the twenty-first century[14,75] (Fig. 4b, SSP3-7.0 and SSP5-8.5). Over the coming two-to-three decades, the summer-positive SAM trend is projected to get weaker under all emission scenarios owing to the opposing influence of stratospheric ozone recovery and increasing greenhouse gases[14]. By the second half of the twenty-first century, the SAM is likely to shift to a positive state across all seasons under the high (SSP3-7.0) and very high (SSP5-8.5) emission scenarios (Fig. 4b).

Conversely, the very low (SSP1-2.6) and low (SSP2-4.5) emission scenarios indicate stabilization of the SAM by 2045–2055, followed by slightly negative SAM trends that begin to return SAM back towards the historical state by the end of the century[14,75] (Fig. 4b). These insights highlight that large-scale emissions reductions could reverse the positive SAM trend. The 1,000-year ACCESS-ESM-1.5 simulations that have been run under net-zero emissions scenarios[76] for warming ranging from 1.6 °C to 3.3 °C at a rate of 0.03–0.05 °C per century indicate a very weak tendency towards negative SAM over a millennium (Fig. 4c). Most land regions are projected to cool after emissions cessation. However, continued warming of the surface Southern Ocean even after emissions cessation is expected to cause global average sea surface temperatures to continue to increase[76], driving ongoing global warming even under net-zero emissions[77]. As the climate adjusts to a new equilibrium characterized by warming of the Southern Ocean and a reduced meridional temperature gradient across the Southern Hemisphere, SAM trends are likely to reverse relative to the current transient warming climate, with consequences for mid-latitude and high-latitude climates[78,79].

Ocean and cryosphere impacts of SAM

This section outlines the influence of the SAM on ocean circulation, the cryosphere and marine biogeochemistry across the Southern Hemisphere[13,80,81]. The SAM strongly influences the frequency of mid-latitude weather systems that form the Southern Hemisphere storm track. Positive SAM is associated with increased cyclone frequency around the Antarctic coastline (~65° S) and more frequent

anticyclones at ~40° S; together these changes are consistent with dipole changes in MSLP during positive SAM[82–87]. During negative SAM, decreased MSLP between 40° S and 50° S is associated with an increase in the frequency of fronts that extend from their parent cyclone[80,85,88] due to increased cyclone frequency at ~50° S. The relationship between the SAM and the frequency of weather systems implies that the SAM affects temperature and rainfall across the Southern Hemisphere (Fig. 6a–d). By modulating the mid-latitude westerly jet, the SAM also exerts a substantial influence on Southern Ocean circulation and sea ice coverage (Fig. 6e,f).

Southern Ocean circulation

There is substantial uncertainty regarding the response of the zonal Antarctic Circumpolar Current to long-term positive SAM trends. Previous climate models suggested that the Antarctic Circumpolar Current transport should increase in response to the positive SAM trend[89–95]. However, observations and idealized high-resolution ocean model simulations indicate that the net Antarctic Circumpolar Current transport is insensitive to changes in zonal wind stress associated with changes in SAM, due to eddy saturation[96–99]. Instead, the additional energy from increased zonal winds enhances the mesoscale eddy field[97–100].

The surface mid-latitude westerly jet has an important role in driving the local and global meridional ocean circulation. At mid–high latitudes, westerly winds drive strong northwards Ekman transport, with the resulting ocean divergence north of the Antarctic continental shelf causing upwelling of warm Circumpolar Deep Water (Fig. 7a). This Ekman transport steepens density surfaces (isopycnals), whereas enhanced mesoscale eddy activity flattens the isopycnals (eddy compensation)[99]. This balance shapes the upper branch of the Southern Ocean meridional overturning circulation[101]. Additionally, around the Antarctic margins, the SAM has also been shown to influence the lower cell of the meridional overturning circulation. The lower cell is influenced by the formation rates of the Ross Sea and Cape Darnley dense shelf waters (precursors to Antarctic Bottom Water production), which are positively correlated with the zonal wind stress, and hence the SAM[102,103].

It has been hypothesized that the Southern Ocean surface could exhibit a two-timescale response to a sustained positive SAM[104,105]. In the high-latitude Southern Ocean, cool surface waters overlay warm Circumpolar Deep Water. At short timescales, enhanced northwards Ekman transport caused by a positive SAM is associated with surface cooling (Fig. 7a). Over time, prolonged positive SAM results in increased Ekman upwelling of warm Circumpolar Deep Water into the surface layer, resulting in surface warming[105]. This two-timescale response could explain the changes in the Southern Ocean surface temperatures since the 1980s with temperatures decreasing during 1980–2010 but subsequently increasing[106,107]. There are many questions about the two-timescale hypothesis. First, the timing of the two-timescale response is highly uncertain, with modelled estimates ranging from 3 to 25 years to transition from surface cooling to warming, and, in some cases, the transition never occurring[105,108,109]. The estimated timescales from models are highly dependent on the specific model characteristics, including horizontal resolution and ocean stratification. Additionally, higher-resolution ocean models suggest that the increase in upwelling is substantially reduced by eddy compensation[110]. Second, although the initial cooling is robust in observations[111] and models[109,112], this cooling is not only driven by Ekman transport but also includes atmospheric drivers and ocean mixing[112,113]. Thus, further evaluation is needed to confirm the real-world impact of the two-timescale response.

Some physical mechanisms of how the SAM will affect Southern Ocean circulation throughout the twenty-first century are reasonably well understood, but a robust projection is still elusive, mainly owing to uncertainty in the eddy field response. There is broad agreement across models that a sustained positive SAM over the twenty-first century will drive an increased meridional overturning circulation[99]; however, there are large uncertainties regarding the effect of a changing mesoscale eddy field on the strength and vertical structure of this response (Fig. 7a). Further, sea ice-related freshwater fluxes influence Southern Ocean circulation[114,115] but their role in mediating the response to the SAM, including on dense shelf water production, has not yet been explored. Thus, the response of ocean circulation to a sustained positive SAM trend over the twenty-first century could be affected by wind-driven changes and sea ice changes, the latter of which are currently poorly represented in climate models. Additionally, further work is needed to explore how a long-term weakly negative SAM under net-zero emissions might affect Southern Ocean circulation.

Antarctic sea ice

The responses of regional sea ice to the SAM exhibit substantial variability. During positive SAM, strengthened surface westerly winds drive the northwards Ekman drift in sea ice, pushing the ice edge northwards and increasing the total sea ice extent. However, the response of sea ice to the SAM varies between regions and with the season[93,94] (Fig. 6e,f). Meridional winds, specifically winds normal to the ice edge, have a stronger impact on sea ice extent than zonal winds[116–118]. The Amundsen Sea Low drives meridional winds, causing a dipole pattern in sea ice response: poleward winds limit sea ice in the Weddell and Bellingshausen seas and equatorward winds increase ice cover in the Amundsen and Ross seas[119] (Fig. 6f). As such, SAM asymmetry and the Amundsen Sea Low have a disproportionately large impact on West Antarctic sea ice coverage[30,119,120]. Despite having regionally varying impacts on sea ice, summer-positive SAM is associated with increased sea ice in most regions, except around the Antarctic Peninsula (Fig. 6e). Research on the SAM impact on sea ice has been primarily focused on surface winds; however, climate models suggest that increased cloud cover and precipitation associated with positive SAM also contribute to increased sea ice coverage[121], albeit to a lesser extent.

There has been much interest in the contribution of the SAM to the evolution of sea ice coverage. Since regular satellite records began in the late 1970s, Antarctic sea ice coverage (as measured by sea ice area and extent) underwent a sustained positive trend until 2014, followed by a sudden drop in 2015–2016, and has been in a sustained low state since then[107,122]. An unusually negative SAM is widely thought to have been a factor in the notable loss of sea ice in November to December 2016 (refs. 123,124). However, very low sea ice summers then occurred in 2022, 2023 and 2024 during positive SAM[107]. Emerging evidence points to large late-winter to early spring variations in the SAM contributing to declines in the Antarctic sea ice area since 2016 (ref. 125), noting that extreme winter declines since 2023 have been strongest in early mid winter[107].

Although overall sea ice coverage is expected to increase with positive SAM, coupled climate models show decreased Antarctic sea ice cover in response to a sustained positive SAM[126]. This disparity might be explained by differences in the two-timescale response hypothesis[105],

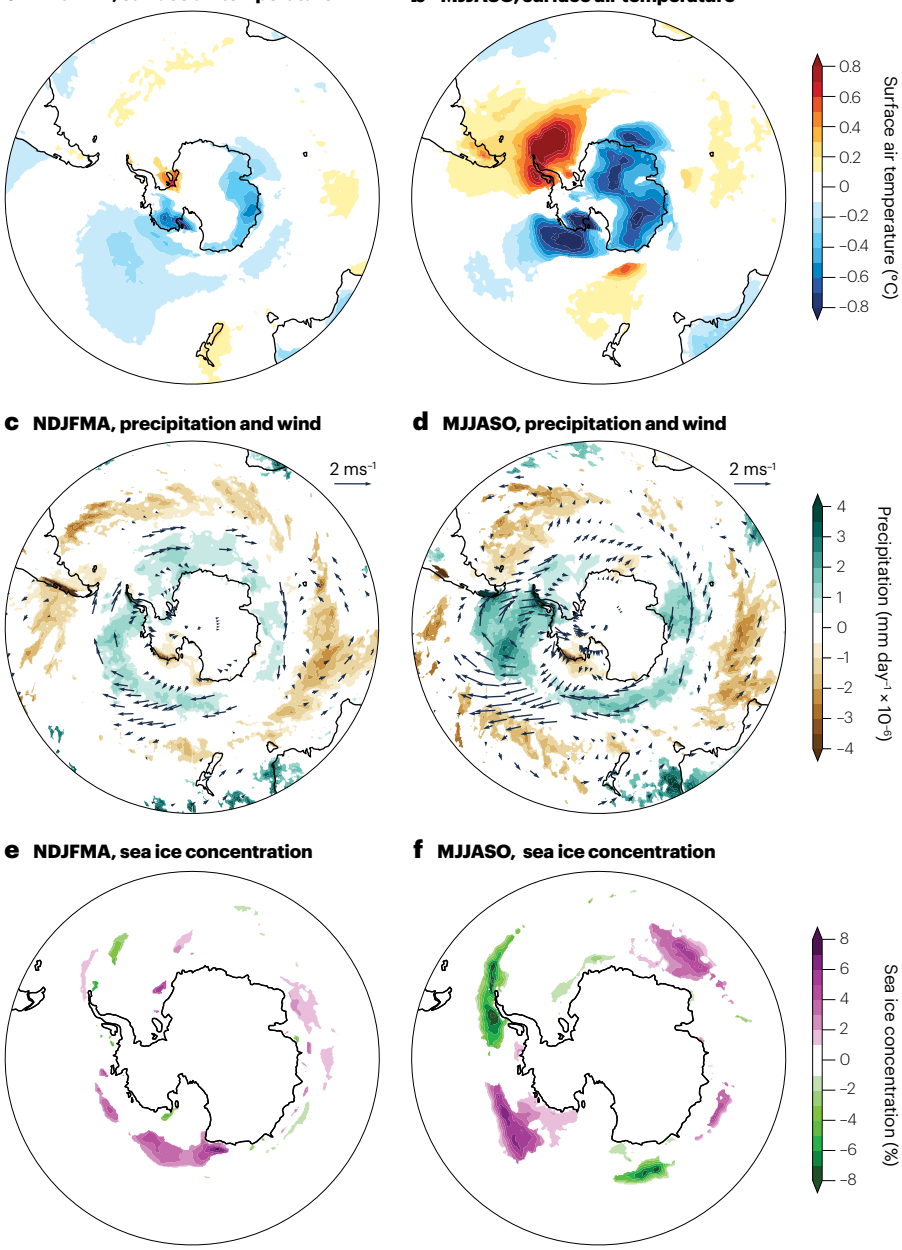

Fig. 6 | Seasonal surface impacts of the SAM. **a**, Regression of the austral warm season (November to April; NDJFMA)-averaged monthly Southern Annular Mode (SAM) index onto surface air temperature[201] over 1979–2023. **b**, As in panel **a** but for the austral cool season (May to October; MJJASO). **c**,**d**, As in panels **a** and **b** but for precipitation[201] and 850-hPa winds[201]. **e**,**f**, As in **a** and **b** but for sea ice concentration[200]. Regressions that do not reach 90% statistical significance have been masked out. Through its impact on atmospheric circulation, SAM affects surface temperature, precipitation and sea ice concentration, with clear regional effects associated with the asymmetric component of SAM.

and/or by changes in mixing between the deep ocean and mixed layer and the associated vertical heat fluxes[113]. Despite its strong influence on regional sea ice variability and trends, the SAM appears to have a very limited impact on the total Antarctic sea ice area[127,128] and is unlikely to have driven historical sea ice trends[127].

The sensitivity of sea ice to SAM asymmetry has implications for the future of Antarctic sea ice. The traditional dipole sea ice response to positive SAM (more sea ice in the Amundsen Sea compensated by less sea ice near the peninsula; Fig. 6f) means that over the satellite era, the net SAM response of the circumpolar sea ice area has been small. However, the sensitivity of sea ice to the SAM might change with projected changes in SAM asymmetry. Furthermore, the influence of the changing seasonality of SAM trends — shifting from summer intensified during the ozone-depletion era to year round by the late twenty-first century — on sea ice remains uncertain.

High-latitude ocean and ice shelves

Mass loss from the Antarctic Ice Sheet is an important contributor to global sea level rise and is the largest source of uncertainty in projections of future sea level[14,129]. Mass loss from the Antarctic Ice Sheet accelerated over 1992–2020, contributing to 5–15% of the observed global sea level rise during this time[130]. Floating ice shelves buttress the land-based ice sheet, so that ice shelf basal melting — which can be mediated by the strength and position of the

mid-latitude westerly jet, and thus the SAM — can indirectly affect the rate of mass loss.

Around the Antarctic margins, positive SAM weakens the Antarctic Slope Current and the coastal currents, enabling more warm Circumpolar Deep Water to flow onshore[131,132]. The currents on and along the Antarctic slope and coast are the primary barriers to the transport of ocean heat towards the Antarctic ice shelves (Fig. 7a). Ocean melting of these ice shelves has a critical role in mediating the contribution of Antarctica to sea level rise[133]. The heat content of the Antarctic shelf waters has increased since the 1970s, especially in West Antarctica[134,135]. This increase is in part due to enhanced westerly winds, as continental shelf winds drive the transport of ocean heat[133,136] on the shelf and basal melting, particularly at several rapidly thinning ice shelves in the Antarctic Peninsula and Amundsen Sea[137,138]. The positive SAM trend is linked with strengthened westerly wind stress or weakened high-latitude easterly wind stress over the continental slope and shelf regions (Fig. 6c,d). These winds favour the upwelling of Circumpolar Deep Water onto the continental shelf and might cause warming at ice cavity depths[131,139–141] (Fig. 7a). However, the cavity response is regional and depends on local wind-driven vertical mixing and surface buoyancy fluxes[131,139–141].

Historical and future changes in the SAM affect the latitude and strength of the zonal winds near the Antarctic coast. Positive SAM shifts ocean circulation features southwards, modifying how the ocean and ice shelves interact, for example, by bringing regions of upwelling warm deep water closer to the continental shelf[142,143]. Even in regions where these latitude shifts have not directly affected the ocean circulation, changes initiated by wind perturbations can propagate around the Antarctic coastline, possibly leading to effects in distant coastal locations[144]. Anthropogenic forcings caused the shelf-break winds in the Amundsen Sea to transition from easterlies in the 1920s to the present near-zero zonal-mean zonal winds, leading to persistent intrusions of warm ocean water onto the continental shelf[145]. Additionally, positive SAM trends driven by greenhouse gas emissions lead to a decrease in the historical and projected strength of near-Antarctic easterly winds[145–148].

The projected sustained positive SAM will strongly influence the temperature on the continental shelf throughout the twenty-first century. Increased transport of warm Circumpolar Deep Water onto the continental shelf caused by the positive SAM phase is likely to be detrimental to Antarctica's ice shelves by increasing basal melt of the shelves. Wind-driven shifts in the intensity or position of the Antarctic slope current will modify the temperature of the water on the shelf and therefore exert a strong influence over the heat budget of the Antarctic margins.

Antarctic Ice Sheet

The SAM can affect Antarctic mass changes via the ocean (as described above), and via more direct atmospheric processes. By influencing the large-scale atmospheric circulation and moisture flux towards the Antarctic continent, SAM affects the surface mass balance of the Antarctic Ice Sheet (Fig. 7a). The Antarctic temperature response to the SAM is broadly spatially consistent, except over the Antarctic Peninsula (Fig. 6a,b). Positive SAM is associated with anomalously warm conditions over the Antarctic Peninsula and cool conditions across West and East Antarctica[149–151]. The magnitude of this response is strongest (0.4–0.8 °C) in the cool season (Fig. 6b). Negative SAM is linked to elevated summer temperature across West and East Antarctica, and increased surface meltwater on ice shelves[152].

The relationship between the SAM and Antarctic precipitation is spatially heterogeneous[153] (Fig. 6c,d). Positive SAM is associated with increased precipitation over the Antarctic Peninsula, and decreased precipitation over the Amundsen coast of West Antarctica (Fig. 6c,d). As with temperature, the strength of the precipitation response to the SAM phase is strongest in the cool season. However, there is high uncertainty in the response of Antarctic precipitation to the SAM owing to the lack of good-quality, long-term precipitation records over the continent[154]. Analysis covering 1979–2013 identified increased precipitation over the Antarctic Peninsula in association with positive SAM, but also included decreased precipitation over East Antarctica[155], which is not apparent for 1979–2023 (Fig. 6c,d). This difference highlights the uncertainty in the response of Antarctic precipitation to SAM. Further, Antarctic precipitation variability is marked by standalone events such as extreme precipitation events, which are linked to atmospheric river events[156]. Negative SAM is associated with an increased frequency of extreme precipitation events owing to increased Rossby wave breaking on the poleward side of the mid-latitude westerly jet[157]. Therefore, the negative SAM is often associated with atmospheric rivers[151,155,156,158]; however, this relationship is weak and regionally specific[156].

The influence of the positive SAM trend on surface mass balance and ice sheet variability since the 1980s remains unclear. Since the 1990s, Antarctic surface mass balance has shown no significant trend (owing to large interannual variability), whereas Antarctic Ice Sheet mass balance has declined[130,159]. Climate models suggest that ozone depletion and the positive summer SAM trend over the late twentieth century were associated with increased precipitation and surface mass gain over West and East Antarctica[12,159,160] over the second half of the twentieth century. Conversely, ice core accumulation records suggest that the positive SAM trend reduced net precipitation accumulation[161]. These diverging results could be related to the offset seasonal response between the summer SAM trend and dominant cool season precipitation. Further, the increase in snowfall accumulation across Antarctica has been explained by synoptic-scale processes[162], rather than the annual-mean SAM trend, which probably primarily reflects the summer trend in the SAM over the satellite era. Therefore, it is important to examine the influence of the projected year-round positive SAM trend on Antarctic surface mass balance over the twenty-first century.

Timescales of ice sheet variability are much longer than those of SAM variability. Comparing the SAM and ice sheet interannual variability suggests that the SAM has minimal influence on Antarctic Ice Sheet mass change[163,164]. However, using trends or cumulative SAM indices identified periods of prolonged positive and negative SAM influence on Antarctic Ice Sheet variability, primarily through precipitation changes[165,166]. The percentage of ice sheet variability explained by the cumulative SAM varies from 55% for West Antarctica[166] (with minimal SAM influence in East Antarctica and the Peninsula) to 67–72% for the total ice sheet[165]. More pertinently, potentially ~40% of the total Antarctic ice loss during 2002–2021 is attributed to the prolonged positive SAM[166]. However, cumulative time series are hard to interpret physically and present a large degree of autocorrelation, and the observational record of Antarctic Ice Sheet balance is very short, so more research is needed.

Southern Ocean biogeochemistry

The effects of the SAM on Southern Ocean circulation are globally important because the Southern Ocean has an outsized role in the global carbon cycle[167]. The Southern Ocean is the largest oceanic sink of anthropogenic carbon, representing approximately 43 ± 3% of the global uptake of anthropogenic carbon by oceans[167]. This region is also an important source of natural CO_2 to the atmosphere, as it is upwelled

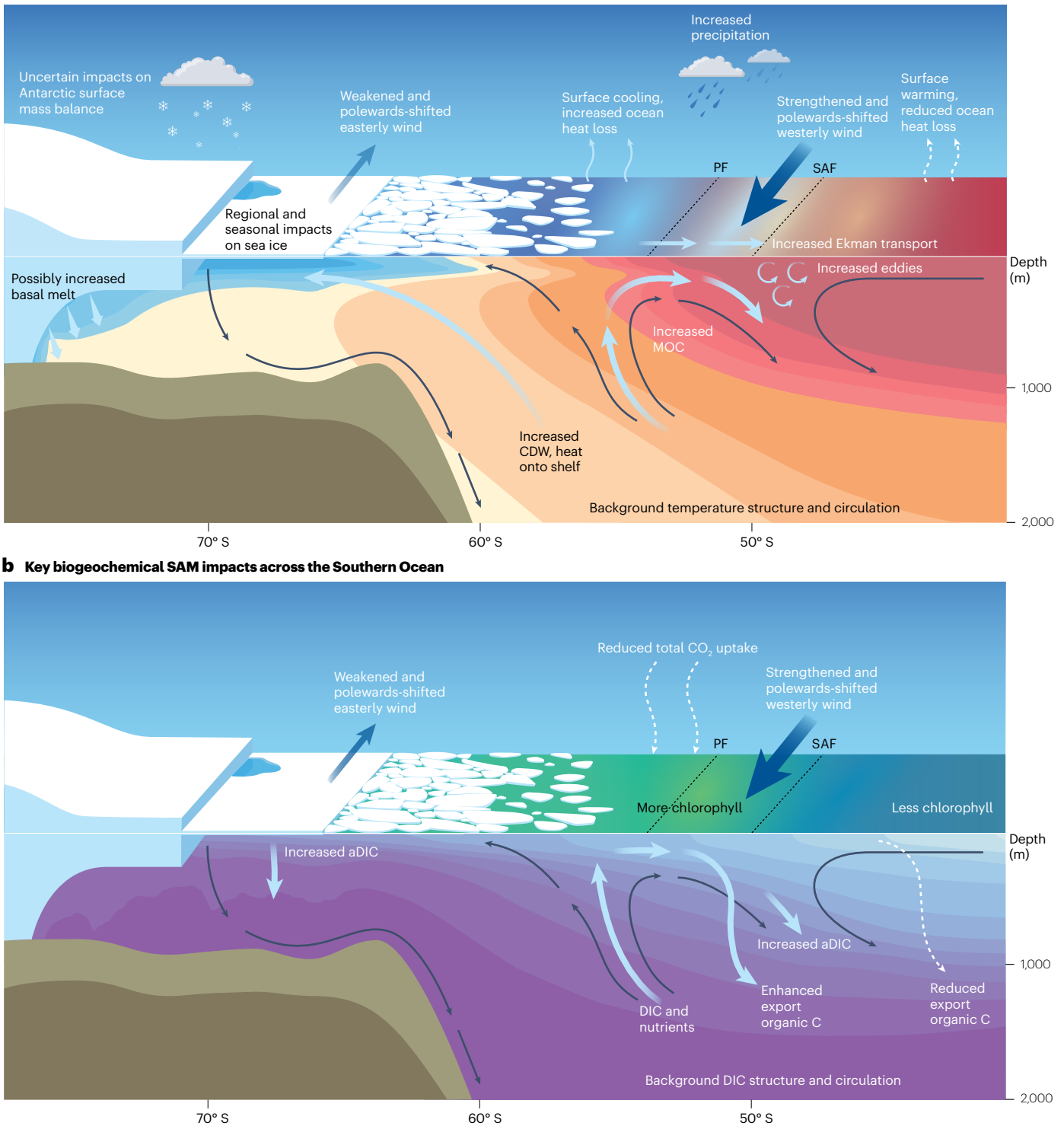

Fig. 7 | Key physical and biogeochemical impacts of SAM. a, A schematic representation of the key physical effects of a positive Southern Annular Mode (SAM) across the Southern Ocean and Antarctica. **b**, As in panel **a** but for biogeochemical effects. In the ocean, thin dark blue arrows represent the mean-state circulation and carbon and nutrient transport; the thick light blue arrows represent changes associated with positive SAM. The SAM affects the physical and biogeochemical state of the Southern Ocean, and thus heat and carbon fluxes, through its change in oceanic circulation. aDIC, anthropogenic dissolved inorganic carbon; CDW, Circumpolar Deep Water; DIC, dissolved inorganic carbon; MOC, meridional overturning circulation; PF, polar front; SAF, sub-Antarctic front.

and outgassed by the mean-state circulation. These processes are mediated by variability and changes in the SAM (Fig. 7b).

Total CO_2 uptake in the Southern Ocean has exhibited a large decadal-scale variability since the 1980s[168], mostly owing to changes in natural CO_2 uptake[169]. Enhanced oceanic upwelling of natural carbon during positive SAM increases outgassing of carbon to the atmosphere by up to 0.2 GtC yr^{-1} (Fig. 7b). Positive SAM increases surface dissolved inorganic carbon south of the polar front[170–172] and deepens the mixed layer[173], increasing the vertical flux of dissolved inorganic carbon at the base of the mixed layer[174]. These processes increase the dissolved inorganic carbon concentration and partial CO_2 pressure of the surface waters, increasing the outgassing of natural carbon to the atmosphere south of the polar front[170–172,174,175].

Positive SAM also affects the uptake of Southern Ocean anthropogenic CO_2. A deepened mixed layer, in association with higher rates of subduction and bottom water formation resulting from positive SAM (Fig. 7a), enhances the uptake of anthropogenic CO_2 and the entrainment of anthropogenic dissolved inorganic carbon in the ocean[169,171,175–177] (Fig. 7b). However, this enhanced uptake of anthropogenic CO_2 is equivalent to about 30% of the outgassing of natural CO_2 (refs. 171,175). Hindcast simulations suggest that total Southern Ocean CO_2 uptake is reduced by 0.1–0.2 GtC yr^{-1} during positive SAM because natural CO_2 outgassing exceeds the uptake of anthropogenic CO_2 (refs. 171,175). However, observations integrated over the whole Southern Ocean suggest that the SAM does not affect total CO_2 uptake[178]. This difference between modelled and observed trends could be attributed to an increase in Southern Ocean surface buoyancy throughout the twenty-first century resulting from increased surface warming and freshening[179,180]. Southern Ocean carbon fluxes are dependent on the stratification of the Southern Ocean; therefore, the increased surface buoyancy could provide a compensating negative feedback to the wind-driven SAM-related carbon fluxes.

Ocean circulation changes driven by the SAM affect Southern Ocean biogeochemistry beyond carbon. The overturning circulation response to positive SAM increases the subduction of nutrients into mode and intermediate waters, with flow-on effects to productivity at lower latitudes[181]. The SAM also affects the depth of the mixed layer, which in turns affects phytoplankton growth[173]. For example, during positive SAM, the mixed layer deepens by up to 100 m in the eastern Indian Ocean and the central Pacific Ocean north of the polar front, reducing chlorophyll concentrations by up to 0.02 mg m^{-3} owing to reduced light availability[173]. Additionally, SAM-induced upwelling south of the polar front alleviates the iron limitations on productivity[182], increasing surface chlorophyll by up to 0.1 mg m^{-3} for a one standard deviation SAM increase[183], albeit with some seasonal and spatial asymmetry[184], leading to increased carbon uptake[172] (Fig. 7b). The composition of under-ice phytoplankton communities is also sensitive to the SAM owing to the effect of the SAM on sea ice seasonality[185]. Towards the equator, SAM-induced circulation changes lead to convergence around the sub-Antarctic front, reducing productivity and thus carbon uptake[172,183].

As the SAM continues its positive trend over the twenty-first century, the capacity of the Southern Ocean to take up carbon is likely to decrease. Meltwater input from Antarctica is also projected to weaken the lower overturning cell by about 40% by 2050 (ref. 186). This weakening would affect the Southern Ocean biogeochemical response by increasing stratification and reducing both the uptake of anthropogenic carbon and outgassing of natural carbon. The net effect on contemporary carbon will, however, depend on many factors, including carbon emissions and surface ocean warming, and will thus need to be studied in detail.

Summary and future perspectives

Positive trends in the SAM since the mid-twentieth century are unprecedented over the last millennium[57]. These trends are particularly strong in austral summer owing to ozone depletion during the 1970s to 1990s (ref. 51) with a year-round contribution from increasing greenhouse gases[63]. A year-round positive trend in the SAM is projected to continue over the twenty-first century under high to very high emissions pathways[14], whereas stabilization due to the competing effects of ozone recovery and increasing greenhouse gases is found in lower emission pathways. Further work is needed to refine how the SAM will change under net-zero and net-negative emissions pathways. The effects of the SAM on Southern Ocean circulation[131], ice shelf melt, meridional moisture transport and Antarctic snow accumulation[166] will have long-term implications on Antarctic mass changes and thus sea level rise. Therefore, an improved understanding of the SAM and its projected effects are needed to inform climate adaptation over the twenty-first century and beyond.

Improved theory, models and modelling systems are needed to better simulate and understand the SAM and its connections with the polar vortex, weather systems, tropical teleconnections and the cryosphere. Such developments could include the incorporation of coupling between dynamics and chemistry, and increased horizontal and vertical model resolution in the atmosphere and ocean[187,188]. Research suggests a link between the SAM and sea surface temperature trends in the tropical Pacific Ocean, with stronger winds over the Southern Ocean leading to cooler sea surface temperature in the Southern Ocean, which subsequently affects sea surface temperatures in the tropical eastern Pacific[189]. Thus, improved representation of the SAM and its effects could also improve simulations of tropical Pacific trends[188].

There is growing recognition that the SAM comprises zonally symmetric and asymmetric components. Although coupled models represent the symmetric component of the SAM well, they do not accurately represent the asymmetric component[190]. This model deficiency has implications for the simulation of SAM teleconnections sensitive to the asymmetric component, for example, across eastern Australia[80,191], southeastern South America[25,81,192,193] and around Antarctica[116–118]. The strengthening of the asymmetric component of the SAM over the satellite era[24,25,32] further motivates the need for improved representation of SAM asymmetry.

A better understanding of the competing influences of stratospheric ozone recovery and continued greenhouse gas increases on the SAM and the implications for changed seasonality in SAM trends is required to better interpret Southern Hemisphere climate projections. Hist-stratO3 experiments use prescribed ozone to isolate the effect of ozone depletion on the climate; however, this approach leads to a mismatch between atmospheric dynamics and chemistry[61,187]. Experiments without interactive stratospheric chemistry can erroneously attribute the relative importance of individual forcings to SAM trends[61]. Furthermore, the inclusion of tropospheric ozone (included in most previous prescribed ozone experiments but not in CMIP6) and ozone depleting substances (included in Chemistry–Climate Model Initiative experiments) can complicate the attribution to stratospheric ozone alone. Designing experiments to separate these various anthropogenic forcings in the presence of internal variability is thus critical to inform future projections of the SAM. Large-ensemble single-forcing experiments are underway that could enable a more complete attribution of anthropogenic forcing on the SAM and its regional effects[194].

Glossary

Amundsen Sea Low
A climatological persistent low-pressure centre located in the Pacific sector of the Southern Ocean off the coast of West Antarctica, over the Amundsen and Bellingshausen seas.

Antarctic Bottom Water
A cold, dense water mass formed near Antarctica from dense shelf water that sinks and spreads along the ocean floor into the deepest parts of the global ocean; it has a key role in global meridional ocean circulation and climate regulation.

Antarctic Circumpolar Current
A major eastwards-flowing ocean current that encircles Antarctica, connecting the Atlantic, Indian and Pacific oceans, thereby facilitating the global exchange of heat, freshwater and nutrients.

Antarctic Slope Current
A high-latitude westwards-flowing current on the edge of the Antarctic continental shelf that encircles most of the continent and forms a boundary between the open ocean and continental shelf waters, regulating the transport of water towards the continent.

Antarctic stratospheric vortex
A band of strong winds blowing from the west to the east, encircling the mid-latitude to sub-Antarctic region in the stratosphere (~10–55 km altitudes), typically present from austral late autumn to late spring.

Anthropogenic carbon
Carbon within the atmospheric, oceanic or terrestrial realm that is of anthropogenic origin.

Chlorophyll
The photosynthetic pigment contained in land plants and ocean phytoplankton, used here as a proxy for phytoplankton abundance and, approximately, ocean productivity.

Circumpolar Deep Water
A water mass that upwells to the near surface of the polar and subpolar Southern Ocean, consisting of a blend of deep water masses from the Atlantic, Indian and Pacific ocean basins, with about half sourced from North Atlantic deep water.

Coupled Model Intercomparison Project phase 6
(CMIP6). The internationally coordinated set of defined climate model experiments and shared model outputs from modelling groups around the world.

Dense shelf water
A dense water mass formed on the Antarctic continental shelf through sea ice production whose temperature is therefore the local freezing temperature and its density is set by its salinity.

Dissolved inorganic carbon
The sum of bicarbonate (HCO_3^-) and carbonate (CO_3^{2}) ions, plus aqueous CO_2 ($CO_{2(aq)}$), also referred to as carbonic acid, H_2CO_3.

Eddy
A transient disturbance that deviates from the mean flow in the atmosphere or ocean (includes cyclones and anticyclones in the atmosphere).

Eddy momentum flux convergence
The net transfer of zonal momentum from atmospheric eddies into the mean flow, resulting in westerly acceleration of the zonal-mean flow caused by the propagation of waves away from their source region.

Eddy momentum flux divergence
The net removal of zonal momentum from the mean flow by atmospheric eddies, corresponding to deceleration of the zonal-mean flow due to breaking waves.

Ekman transport
Also termed Ekman drift; a wind-driven flow of water in the upper surface layer of the ocean resulting from a combination of wind drag and the Coriolis effect, which deflects the flow to the left of the wind in the Southern Hemisphere, and to the right of the wind in the Northern Hemisphere.

El Niño Southern Oscillation
(ENSO). A naturally occurring fluctuation in sea surface temperatures coupled with winds and pressure across the tropical Pacific Ocean, associated with sustained warming (El Niño) or cooling (La Niña) in the central and eastern tropical Pacific, typically occurring every 2–7 years.

Ferrel cell
The mid-latitude component of the extratropical mean meridional circulation, consisting of poleward flow near the surface, upwards motion near the mid-latitude jet, equatorward flow aloft and subsidence in the subtropics.

Hadley circulation
Also termed Hadley cell; the thermally driven mean meridional circulation characterized by rising warm, moist air in the tropics; poleward motion aloft; sinking cooler, drier air in the subtropics; and equatorward flow at the surface, transporting energy, momentum and moisture between these regions.

Interdecadal Pacific Oscillation
A naturally occurring decadal-to-multidecadal fluctuation of Pacific sea surface temperatures, coupled with atmospheric circulation, with a spatial pattern resembling ENSO but extending into the extratropical Pacific.

Madden–Julian Oscillation
A pulse of tropical convective activity (cloud and rainfall) that propagates eastwards near the equator, from the Indian Ocean to the western Pacific Ocean, with a cycle repeating approximately every 30–60 days.

Mid-latitude eddy-driven jet
A band of strong westerly winds extending from the surface to the upper troposphere in the mid-to-high latitudes of both hemispheres, driven by eddy momentum flux convergence. Unlike the subtropical jet, the mid-latitude eddy-driven jet arises from the cumulative effect of eddies rather than a coherent flow.

Natural carbon
Carbon within the atmosphere, oceanic or terrestrial realm that has not been affected by anthropogenic emissions of carbon, considered equivalent to pre-industrial carbon.

Net-zero emissions
The balance of anthropogenic carbon dioxide emissions with equivalent uptake of carbon from the atmosphere through anthropogenic activities (sometimes net-zero emissions are used to refer to all greenhouse gases rather than just carbon dioxide).

Pacific–South American pattern
A Rossby wave train that extends from the central Pacific Ocean to the Amundsen and Weddell seas, manifesting across intraseasonal to decadal timescales.

Rossby waves
Large-scale (planetary) or synoptic-scale waves in the atmosphere that arise from the variation of the Coriolis effect with latitude.

Subtropical jet
A band of strong westerly winds located in the upper troposphere of the subtropics on the poleward side of the Hadley cell of both hemispheres, peaking in winter.

Surface mass balance
The net effect of ice sheet mass gain due to precipitation, and mass loss primarily by temperature-driven surface melt.

Understanding the interplay between the atmosphere and ocean as drivers of the exceptionally low Antarctic sea ice cover is a topic of much interest. There is low confidence in the ability of models to project the response of the Southern Ocean and sea ice to a changing SAM[129], owing to known model deficiencies, such as the Southern Ocean cloud-related radiative bias[195] and representation of ocean mixing[196]. Ongoing monitoring of the subsurface Southern Ocean and field campaigns will help to investigate these problems. Efforts to explore the contribution of prolonged positive SAM and increased Ekman upwelling to surface and subsurface ocean warming will strengthen understanding of the interconnections between the atmosphere, ocean and sea ice, and improve projections of future sea ice and Southern Ocean changes.

The SAM also has a fundamental role in setting the surface mass balance of Antarctica's ice sheets, by regulating coastal winds, snowfall rates and regional air temperatures. Reconciling the multiple approaches examining the drivers of Antarctic surface mass balance in the observational record and Earth system models is critical to understanding past, present and projected changes of Antarctic surface mass balance. Yet understanding of the processes linking the SAM to Antarctic coastal climate variability is limited, with little known, for example, about how the SAM interacts with katabatic winds, or how these interactions might link with changing Antarctic margin conditions. Process-based studies that resolve these interactions are needed, combining available observations and high-resolution model simulations. Additionally, the effect of SAM on Antarctic margin ocean circulation, properties and ice shelf melting is poorly understood, although this probably varies regionally, depending on local ocean conditions, shelf circulation and ice cavity geometry. Therefore, a targeted examination of individual cavity systems is needed to understand the cumulative effect of projected SAM changes on Antarctic ice shelves. In addition, more research is needed to understand how the SAM will influence Antarctic surface mass balance throughout the twenty-first century. Ultimately, this requires the development of Earth system models that properly integrate Antarctica's ice sheets and ice shelves in a truly coupled framework.

Data availability

Figures 1–6 were made using data from ERA5 (ref. 197), which is available at https://www.ecmwf.int/en/forecasts/dataset/ecmwf-reanalysis-v5. Figures 1c and 4b used the Marshall SAM index[4], which is available at http://www.nerc-bas.ac.uk/icd/gjma/sam.html. Figure 1c also used the US National Oceanographic and Atmospheric Administration Antarctic Oscillation[198], which is available at https://www.cpc.ncep.noaa.gov/products/precip/CWlink/daily_ao_index/aao/aao.shtml. Figures 4 and 5 were made using CMIP6 data[198] available from the Earth System Grid Federation https://aims2.llnl.gov/search. Figure 4a was also made using data from the Paleoclimate Modelling Intercomparison Project phase 3 data[199], which is also available from the Earth System Grid Federation. Figure 4c was made using data from ACCESS-ESM1.5 emissions-driven runs[76], with data available at https://doi.org/10.5281/zenodo.17364274. Figure 5e,f was made using data from the National Snow and Ice Data Center Climate Data Record version 4 sea ice concentration[200], available from https://nsidc.org/data/g02202/versions/4.

Code availability

Analysis code to reproduce Figs. 1–6 is available via Zenodo at https://doi.org/10.5281/zenodo.17393582.

Published online: 02 December 2025

References

1. Thompson, D. W. J. & Wallace, J. M. Annular modes in the extratropical circulation. Part I: month-to-month variability. *J. Clim.* **13**, 1000–1016 (2000).
2. Rogers, J. C. & Loon, H. van Spatial variability of sea level pressure and 500 mb height anomalies over the Southern Hemisphere. *Mon. Weather Rev.* **110**, 1375–1392 (1982).
3. Gong, D. & Wang, S. Definition of Antarctic oscillation index. *Geophys. Res. Lett.* **26**, 459–462 (1999).
4. Marshall Trends in the Southern Annular Mode from observations and reanalyses. *J. Clim.* **16**, 4134–4143 (2003).
5. Hartmann, D. L. & Lo, F. Wave-driven zonal flow vacillation in the Southern Hemisphere. *J. Atmos. Sci.* **55**, 1303–1315 (1998).
6. Ho, M., Kiem, A. S. & Verdon-Kidd, D. C. The Southern Annular Mode: a comparison of indices. *Hydrol. Earth Syst. Sci.* **16**, 967–982 (2012).
7. Wright, N. M., Krause, C. E., Phipps, S. J., Boschat, G. & Abram, N. J. Influence of long-term changes in solar irradiance forcing on the Southern Annular Mode. *Clim. Past* **18**, 1509–1528 (2022).
8. Velasquez-Jimenez, L. & Abram, N. J. Technical note: an improved methodology for calculating the Southern Annular Mode index to aid consistency between climate studies. *Clim. Past* **20**, 1125–1139 (2024).
9. Lim, E.-P. et al. The 2019 Southern Hemisphere stratospheric polar vortex weakening and its impacts. *Bull. Am. Meteorol. Soc.* **102**, E1150–E1171 (2021).
10. Lim, E.-P. et al. Australian hot and dry extremes induced by weakenings of the stratospheric polar vortex. *Nat. Geosci.* **12**, 896–901 (2019).
11. Harris, S. & Lucas, C. Understanding the variability of Australian fire weather between 1973 and 2017. *PLoS ONE* **14**, e0222328 (2019).
12. Lenaerts, J. T. M., Fyke, J. & Medley, B. The Ssgnature of ozone depletion in recent antarctic precipitation change: a study with the community earth system model. *Geophys. Res. Lett.* **45**, 12,931–12,939 (2018).
13. Fogt, R. L. & Marshall, G. J. The Southern Annular Mode: variability, trends, and climate impacts across the Southern Hemisphere. *WIREs Clim. Change* **11**, e652 (2020).
14. IPCC. *Climate Change 2021: The Physical Science Basis. Contribution of Working Group I to the Sixth Assessment Report of the Intergovernmental Panel on Climate Change* (eds Masson-Delmotte, V. et al.) (Cambridge Univ. Press, 2023).
15. Nakamura, H. & Shimpo, A. Seasonal variations in the Southern Hemisphere storm tracks and jet streams as revealed in a reanalysis dataset. *J. Clim.* **17**, 1828–1844 (2004).
16. Lorenz, D. J. & Hartmann, D. L. Eddy–zonal flow feedback in the Southern Hemisphere. *J. Atmos. Sci.* **58**, 3312–3327 (2001).
17. Hendon, H. H., Lim, E.-P. & Nguyen, H. Seasonal variations of subtropical precipitation associated with the Southern Annular Mode. *J. Clim.* **27**, 3446–3460 (2014).
18. Codron, F. Relations between annular modes and the mean state: Southern Hemisphere winter. *J. Atmos. Sci.* **64**, 3328–3339 (2007).
19. Barnes, E. A. & Hartmann, D. L. Dynamical feedbacks of the Southern Annular Mode in winter and summer. *J. Atmos. Sci.* **67**, 2320–2330 (2010).
20. Ding, Q., Steig, E. J., Battisti, D. S. & Wallace, J. M. Influence of the tropics on the Southern Annular Mode. *J. Clim.* **25**, 6330–6348 (2012).
21. Gillett, Z. E., Hendon, H. H., Arblaster, J. M. & Lin, H. Sensitivity of the Southern Hemisphere wintertime teleconnection to the location of ENSO heating. *J. Clim.* **36**, 2497–2514 (2023).
22. Hoskins, B. J. & Ambrizzi, T. Rossby wave propagation on a realistic longitudinally varying flow. *J. Atmos. Sci.* **50**, 1661–1671 (1993).
23. Fan, K. Zonal asymmetry of the Antarctic oscillation. *Geophys. Res. Lett.* **34**, L02706 (2007).
24. Fogt, R. L., Jones, J. M. & Renwick, J. Seasonal zonal asymmetries in the Southern Annular Mode and their impact on regional temperature anomalies. *J. Clim.* **25**, 6253–6270 (2012).
25. Campitelli, E., Díaz, L. B. & Vera, C. Assessment of zonally symmetric and asymmetric components of the Southern Annular Mode using a novel approach. *Clim. Dyn.* **58**, 161–178 (2022).
26. Kidston, J., Renwick, J. A. & McGregor, J. Hemispheric-scale seasonality of the Southern Annular Mode and impacts on the climate of New Zealand. *J. Clim.* **22**, 4759–4770 (2009).
27. Pezza, A. B., Rashid, H. A. & Simmonds, I. Climate links and recent extremes in Antarctic sea ice, high-latitude cyclones, Southern Annular Mode and ENSO. *Clim. Dyn.* **38**, 57–73 (2012).
28. Irving, D. & Simmonds, I. A novel approach to diagnosing Southern Hemisphere planetary wave activity and its influence on regional climate variability. *J. Clim.* **28**, 9041–9057 (2015).
29. Ciasto, L. M., Simpkins, G. R. & England, M. H. Teleconnections between tropical Pacific SST anomalies and extratropical Southern Hemisphere climate. *J. Clim.* **28**, 56–65 (2015).
30. Turner, J., Phillips, T., Hosking, J. S., Marshall, G. J. & Orr, A. The Amundsen Sea Low. *Int. J. Climatol.* **33**, 1818–1829 (2013).
31. Clem, K. R., Renwick, J. A. & McGregor, J. Large-scale forcing of the Amundsen Sea Low and its influence on sea ice and West Antarctic temperature. *J. Clim.* **30**, 8405–8424 (2017).
32. Schroeter, S., O'Kane, T. J. & Sandery, P. A. Antarctic sea ice regime shift associated with decreasing zonal symmetry in the Southern Annular Mode. *Cryosphere* **17**, 701–717 (2023).

33. Baldwin, M. P. & Dunkerton, T. J. Stratospheric harbingers of anomalous weather regimes. *Science* **294**, 581–584 (2001).
34. Thompson, D. W. J., Baldwin, M. P. & Solomon, S. Stratosphere–troposphere coupling in the Southern Hemisphere. *J. Atmos. Sci.* **62**, 708–715 (2005).
35. Byrne, N. J. & Shepherd, T. G. Seasonal persistence of circulation anomalies in the Southern Hemisphere stratosphere and its implications for the troposphere. *J. Clim.* **31**, 3467–3483 (2018).
36. Lim, E.-P., Hendon, H. H. & Thompson, D. W. J. Seasonal evolution of stratosphere–troposphere coupling in the Southern Hemisphere and implications for the predictability of surface climate. *J. Geophys. Res. Atmos.* **123**, 12,002–12,016 (2018).
37. Jucker, M. & Reichler, T. Life cycle of major sudden stratospheric warmings in the Southern Hemisphere from a multimillennial GCM simulation. *J. Clim.* **36**, 643–661 (2023).
38. Ambaum, M. H. P. & Hoskins, B. J. The NAO troposphere–stratosphere connection. *J. Clim.* **15**, 1969–1978 (2002).
39. Baldwin, M. P., Birner, T. & Ayarzagüena, B. Tropospheric amplification of stratosphere–troposphere coupling. *Q. J. R. Meteorol. Soc.* **150**, 5188–5205 (2024).
40. Jucker, M. & Goyal, R. Ozone-forced Southern Annular Mode during Antarctic stratospheric warming events. *Geophys. Res. Lett.* **49**, e2021GL095270 (2022).
41. Hendon, H. H., Lim, E.-P. & Abhik, S. Impact of interannual ozone variations on the downward coupling of the 2002 Southern Hemisphere stratospheric warming. *J. Geophys. Res. Atmos.* **125**, e2020JD032952 (2020).
42. Fogt, R. L., Bromwich, D. H. & Hines, K. M. Understanding the SAM influence on the South Pacific ENSO teleconnection. *Clim. Dyn.* **36**, 1555–1576 (2011).
43. Lu, J., Chen, G. & Frierson, D. M. W. Response of the zonal mean atmospheric circulation to El Niño versus global warming. *J. Clim.* **21**, 5835–5851 (2008).
44. L'Heureux, M. L. & Thompson, D. W. J. Observed relationships between the El Niño–Southern Oscillation and the extratropical zonal-mean circulation. *J. Clim.* **19**, 276–287 (2006).
45. Robinson, W. A. A baroclinic mechanism for the eddy feedback on the zonal index. *J. Atmos. Sci.* **57**, 415–422 (2000).
46. Lim, E.-P., Hendon, H. H. & Rashid, H. Seasonal predictability of the Southern Annular Mode due to its association with ENSO. *J. Clim.* **26**, 8037–8054 (2013).
47. Wilson, A. B., Bromwich, D. H. & Hines, K. M. Simulating the mutual forcing of anomalous high southern latitude atmospheric circulation by El Niño flavors and the Southern Annular Mode. *J. Clim.* **29**, 2291–2309 (2016).
48. Wedd, R. et al. ACCESS-S2: the upgraded bureau of meteorology multi-week to seasonal prediction system. *J. South. Hemisph. Earth Syst. Sci.* **72**, 218–242 (2022).
49. Fogt, R. L. & Bromwich, D. H. Decadal variability of the ENSO teleconnection to the high-latitude South Pacific governed by coupling with the Southern Annular Mode. *J. Clim.* **19**, 979–997 (2006).
50. Yang, D. et al. Role of tropical variability in driving decadal shifts in the Southern Hemisphere summertime eddy-driven jet. *J. Clim.* **33**, 5445–5463 (2020).
51. World Meteorological Organization. *Scientific Assessment of Ozone Depletion: 2022* (WMO, 2022).
52. Matthews, A. J. & Meredith, M. P. Variability of Antarctic circumpolar transport and the Southern Annular Mode associated with the Madden–Julian Oscillation. *Geophys. Res. Lett.* **31**, L24312 (2004).
53. Flatau, M. & Kim, Y.-J. Interaction between the MJO and polar circulations. *J. Clim.* **26**, 3562–3574 (2013).
54. Pohl, B., Fauchereau, N., Reason, C. J. C. & Rouault, M. Relationships between the Antarctic Oscillation, the Madden–Julian Oscillation, and ENSO, and consequences for rainfall analysis. *J. Clim.* **23**, 238–254 (2010).
55. Fauchereau, N., Pohl, B. & Lorrey, A. Extratropical impacts of the Madden–Julian Oscillation over New Zealand from a weather regime perspective. *J. Clim.* **29**, 2161–2175 (2016).
56. Lim, E. P. & Hendon, H. H. Understanding the contrast of Australian springtime rainfall of 1997 and 2002 in the frame of two flavors of El Niño. *J. Clim.* **28**, 2804–2822 (2015).
57. Abram, N. J. et al. Evolution of the Southern Annular Mode during the past millennium. *Nat. Clim. Change* **4**, 564–569 (2014).
58. Dätwyler, C. et al. Teleconnection stationarity, variability and trends of the southern annular mode (SAM) during the last millennium. *Clim. Dyn.* **51**, 2321–2339 (2017).
59. Villalba, R. et al. Unusual Southern Hemisphere tree growth patterns induced by changes in the Southern Annular Mode. *Nat. Geosci.* **5**, 793–798 (2012).
60. King, J., Anchukaitis, K. J., Allen, K., Vance, T. & Hessl, A. Trends and variability in the Southern Annular Mode over the Common Era. *Nat. Commun.* **14**, 2324 (2023).
61. Morgenstern, O. The Southern Annular Mode in 6th Coupled Model Intercomparison Project Models. *J. Geophys. Res. Atmos.* **126**, e2020JD034161 (2021).
62. Thompson, D. W. J. et al. Signatures of the Antarctic ozone hole in Southern Hemisphere surface climate change. *Nat. Geosci.* **4**, 741–749 (2011).
63. Eyring, V. et al. in Climate Change 2021 — The Physical Science Basis (eds Masson-Delmotte, V. et al.) https://doi.org/10.1017/9781009157896.005 (IPCC, Cambridge Univ. Press, 2021).
64. Polvani, L. M., Waugh, D. W., Correa, G. J. P. & Son, S.-W. Stratospheric ozone depletion: the main driver of twentieth-century atmospheric circulation changes in the Southern Hemisphere. *J. Clim.* **24**, 795–812 (2011).
65. Gillett, N. P. & Fyfe, J. C. Annular mode changes in the CMIP5 simulations. *Geophys. Res. Lett.* **40**, 1189–1193 (2013).
66. Son, S.-W. et al. Tropospheric jet response to Antarctic ozone depletion: an update with Chemistry–climate Model Initiative (CCMI) models. *Environ. Res. Lett.* **13**, 054024 (2018).
67. Shaw, T. iffany et al. Emerging climate change signals in atmospheric circulation. *AGU Adv.* **5**, 2024AV001297 (2024).
68. Garfinkel, C. I. et al. Impact of parameterized convection on the storm track and near-surface jet response to global warming: implications for mechanisms of the future poleward shift. *J. Clim.* **37**, 2541–2564 (2024).
69. Lachmy, O. The relation between the latitudinal shifts of midlatitude diabatic heating, eddy heat flux, and the eddy-driven jet in CMIP6 models. *J. Geophys. Res. Atmos.* **127**, e2022JD036556 (2022).
70. Tan, Z. & Shaw, T. A. Quantifying the impact of wind and surface humidity-induced surface heat exchange on the circulation shift in response to increased CO. *Geophys. Res. Lett.* **47**, e2020GL088053 (2020).
71. Banerjee, A., Fyfe, J. C., Polvani, L. M., Waugh, D. & Chang, K.-L. A pause in Southern Hemisphere circulation trends due to the Montreal Protocol. *Nature* **579**, 544–548 (2020).
72. Zheng, F. Slowing down of the summer Southern Hemisphere annular mode trend against the background of ozone recovery. *Atmos. Ocean. Sci. Lett.* **17**, 100375 (2024).
73. Schneider, D. P., Deser, C. & Fan, T. Comparing the impacts of tropical SST variability and polar stratospheric ozone loss on the Southern Ocean westerly winds. *J. Clim.* **28**, 9350–9372 (2015).
74. Fogt, R. L. et al. A twentieth century perspective on summer Antarctic pressure change and variability and contributions from tropical SSTs and ozone depletion. *Geophys. Res. Lett.* **44**, 9918–9927 (2017).
75. Goyal, R., Sen Gupta, A., Jucker, M. & England, M. H. Historical and projected changes in the Southern Hemisphere surface westerlies. *Geophys. Res. Lett.* **48**, e2020GL090849 (2021).
76. King, A. D. et al. Exploring climate stabilisation at different global warming levels in ACCESS-ESM-1.5. *Earth Syst. Dyn.* **15**, 1353–1383 (2024).
77. Chamberlain, M. A., Ziehn, T. & Law, R. M. The Southern Ocean as the climate's freight train — driving ongoing global warming under zero-emission scenarios with ACCESS-ESM1.5. *Biogeosciences* **21**, 3053–3073 (2024).
78. Sniderman, J. M. K. et al. Southern Hemisphere subtropical drying as a transient response to warming. *Nat. Clim. Change* **9**, 232–236 (2019).
79. Grose, M. R. & King, A. D. The circulation and rainfall response in the Southern Hemisphere extra-tropics to climate stabilisation. *Weather Clim. Extrem.* **41**, 100577 (2023).
80. Boschat, G., Purich, A., Rudeva, I. & Arblaster, J. Impact of zonal and meridional atmospheric flow on surface climate and extremes in the Southern Hemisphere. *J. Clim.* **36**, 5041–5061 (2023).
81. Ortiz-Guzmán, V., Jucker, M. & Sherwood, S. Zonal Wavenumber 3 forces extreme precipitation in South America. *J. Clim.* **37**, 3649–3660 (2024).
82. Uotila, P., Vihma, T. & Tsukernik, M. Close interactions between the Antarctic cyclone budget and large-scale atmospheric circulation. *Geophys. Res. Lett.* **40**, 3237–3241 (2013).
83. Grieger, J., Leckebusch, G. C., Raible, C. C., Rudeva, I. & Simmonds, I. Subantarctic cyclones identified by 14 tracking methods, and their role for moisture transports into the continent. *Tellus Dyn. Meteorol. Oceanogr.* **70**, 1–18 (2018).
84. Pepler, A. Projections of synoptic anticyclones for the twenty-first century. *Clim. Dyn.* **61**, 3271–3287 (2023).
85. Rudeva, I. & Simmonds, I. Variability and trends of global atmospheric frontal activity and links with large-scale modes of variability. *J. Clim.* **28**, 3311–3330 (2015).
86. Bernardes Pezza, A., Durrant, T., Simmonds, I. & Smith, I. Southern Hemisphere synoptic behavior in extreme phases of SAM, ENSO, sea ice extent, and southern Australia rainfall. *J. Clim.* **21**, 5566–5584 (2008).
87. Spensberger, C., Reeder, M. J., Spengler, T. & Patterson, M. The connection between the Southern Annular Mode and a feature-based perspective on Southern Hemisphere midlatitude winter variability. *J. Clim.* **33**, 115–129 (2020).
88. Simmonds, I., Keay, K. & Tristram Bye, J. A. Identification and climatology of Southern Hemisphere mobile fronts in a modern reanalysis. *J. Clim.* **25**, 1945–1962 (2012).
89. Saenko, O. A., Fyfe, J. C. & England, M. H. On the response of the oceanic wind-driven circulation to atmospheric CO_2 increase. *Clim. Dyn.* **25**, 415–426 (2005).
90. Oke, P. R. & England, M. H. Oceanic response to changes in the latitude of the Southern Hemisphere subpolar westerly winds. *J. Clim.* **17**, 1040–1054 (2004).
91. Fyfe, J. C. & Saenko, O. A. Simulated changes in the extratropical Southern Hemisphere winds and currents. *Geophys. Res. Lett.* **33**, L06701 (2006).
92. Yin, J. H. A consistent poleward shift of the storm tracks in simulations of 21st century climate. *Geophys. Res. Lett.* **32**, L18701 (2005).
93. Hall, A. & Visbeck, M. Synchronous variability in the Southern Hemisphere atmosphere, sea ice, and ocean resulting from the annular mode. *J. Clim.* **15**, 3043–3057 (2002).
94. Sen Gupta, A. & England, M. H. Coupled ocean–atmosphere–ice response to variations in the Southern Annular Mode. *J. Clim.* **19**, 4457–4486 (2006).
95. Bi, D., Budd, W. F., Hirst, A. C. & Wu, X. Response of the Antarctic circumpolar current transport to global warming in a coupled model. *Geophys. Res. Lett.* **29**, 26-1–26–4 (2002).
96. Böning, C. W., Dispert, A., Visbeck, M., Rintoul, S. R. & Schwarzkopf, F. U. The response of the Antarctic circumpolar current to recent climate change. *Nat. Geosci.* **1**, 864–869 (2008).

97. Tansley, C. E. & Marshall, D. P. On the dynamics of wind-driven circumpolar currents. *J. Phys. Oceanogr.* **31**, 3258–3273 (2001).
98. Munday, D. R., Johnson, H. L. & Marshall, D. P. Eddy saturation of equilibrated circumpolar currents. *J. Phys. Oceanogr.* **43**, 507–532 (2013).
99. Morrison, A. K. & Hogg, A. M.cC. On the relationship between Southern Ocean overturning and ACC transport. *J. Phys. Oceanogr.* **43**, 140–148 (2013).
100. Martínez-Moreno, J. et al. Global changes in oceanic mesoscale currents over the satellite altimetry record. *Nat. Clim. Change* **11**, 397–403 (2021).
101. Rintoul, S. N. G., Alberto C. Rintoul, S. in *Ocean Circulation and Climate — A 21st Century Perspective* Vol. 103, 471–492 (Academic, 2013).
102. Schmidt, C., Morrison, A. K. & England, M. H. Wind- and sea-ice-driven interannual variability of Antarctic Bottom Water formation. *J. Geophys. Res. Ocean.* **128**, e2023JC019774 (2023).
103. Zhang, Z. et al. Evidence for large-scale climate forcing of dense shelf water variability in the Ross Sea. *Nat. Commun.* **15**, 8190 (2024).
104. Marshall, J. et al. The ocean's role in polar climate change: asymmetric Arctic and Antarctic responses to greenhouse gas and ozone forcing. *Philos. Trans. R. Soc. Math. Phys. Eng. Sci.* **372**, 20130040 (2014).
105. Ferreira, D., Marshall, J., Bitz, C. M., Solomon, S. & Plumb, A. Antarctic Ocean and sea ice response to ozone depletion: a two-time-scale problem. *J. Clim.* **28**, 1206–1226 (2015).
106. Dong, Y., Polvani, L. M. & Bonan, D. B. Recent multi-decadal southern ocean surface cooling unlikely caused by Southern Annular Mode trends. *Geophys. Res. Lett.* **50**, e2023GL106142 (2023).
107. Purich, A. & Doddridge, E. W. Record low Antarctic sea ice coverage indicates a new sea ice state. *Commun. Earth Environ.* **4**, 314 (2023).
108. Kostov, Y. et al. Fast and slow responses of Southern Ocean sea surface temperature to SAM in coupled climate models. *Clim. Dyn.* **48**, 1595–1609 (2017).
109. Seviour, W. J. M. et al. The Southern Ocean sea surface temperature response to ozone depletion: a multimodel comparison. *J. Clim.* **32**, 5107–5121 (2019).
110. Doddridge, E. W. et al. Eddy compensation dampens Southern Ocean sea surface temperature response to westerly wind trends. *Geophys. Res. Lett.* **46**, 4365–4377 (2019).
111. Doddridge, E. W. & Marshall, J. C. Modulation of the seasonal cycle of Antarctic sea ice extent related to the Southern Annular Mode. *Geophys. Res. Lett.* **44**, 9761–9768 (2017).
112. Seviour, W. J. M., Gnanadesikan, A. & Waugh, D. W. The transient response of the Southern Ocean to stratospheric ozone depletion. *J. Clim.* **29**, 7383–7396 (2016).
113. Doddridge, E. W., Marshall, J., Song, H., Campin, J.-M. & Kelley, M. Southern Ocean heat storage, reemergence, and winter sea ice decline induced by summertime winds. *J. Clim.* **34**, 1403–1415 (2021).
114. Abernathey, R. P. et al. Water-mass transformation by sea ice in the upper branch of the Southern Ocean overturning. *Nat. Geosci.* **9**, 596–601 (2016).
115. Pellichero, V., Sallée, J.-B., Chapman, C. C. & Downes, S. M. The Southern Ocean meridional overturning in the sea-ice sector is driven by freshwater fluxes. *Nat. Commun.* **9**, 1789 (2018).
116. Raphael, M. N. The influence of atmospheric zonal wave three on Antarctic sea ice variability. *J. Geophys. Res. Atmos.* **112**, 2006JD007852 (2007).
117. Yuan, X. & Li, C. Climate modes in southern high latitudes and their impacts on Antarctic sea ice. *J. Geophys. Res. Ocean.* **113**, 2006JC004067 (2008).
118. Eabry, M. D., Goyal, R., Taschetto, A. S., Hobbs, W. & Sen Gupta, A. Combined impacts of Southern Annular Mode and zonal wave 3 on Antarctic sea ice variability. *J. Clim.* **37**, 1759–1775 (2024).
119. Raphael, M. N. et al. The Amundsen Sea Low: variability, change, and impact on Antarctic climate. *Bull. Am. Meteorol. Soc.* **97**, 111–121 (2016).
120. Hosking, J. S., Orr, A., Marshall, G. J., Turner, J. & Phillips, T. The influence of the Amundsen–Bellingshausen seas low on the climate of West Antarctica and its representation in coupled climate model simulations. *J. Clim.* **26**, 6633–6648 (2013).
121. Seviour, W. J. M., Gnanadesikan, A., Waugh, D. & Pradal, M.-A. Transient response of the Southern Ocean to changing ozone: regional responses and physical mechanisms. *J. Clim.* **30**, 2463–2480 (2017).
122. Parkinson, C. L. A 40-y record reveals gradual antarctic sea ice increases followed by decreases at rates far exceeding the rates seen in the Arctic. *Proc. Natl Acad. Sci. USA* **116**, 14414–14423 (2019).
123. Wang, G. et al. Compounding tropical and stratospheric forcing of the record low Antarctic sea-ice in 2016. *Nat. Commun.* **10**, 13 (2019).
124. Meehl, G. A. et al. Sustained ocean changes contributed to sudden Antarctic sea ice retreat in late 2016. *Nat. Commun.* **10**, 14 (2019).
125. Boehm, C. L., Thompson, D. W. J. & Blanchard-Wrigglesworth, E. The key role of the Southern Annular Mode during the sea-ice maximum for Antarctic sea ice and its recent loss. Commun. Earth Environ. 6, 833 (2025).
126. Sigmond, M. & Fyfe, J. C. The Antarctic sea ice response to the ozone hole in climate models. *J. Clim.* **27**, 1336–1342 (2014).
127. Polvani, L. M. et al. Interannual SAM modulation of Antarctic sea ice extent does not account for its long-term trends, pointing to a limited role for ozone depletion. *Geophys. Res. Lett.* **48**, e2021GL094871 (2021).
128. Hobbs, W. et al. Observational evidence for a regime shift in summer Antarctic sea Ice. *J. Clim.* **37**, 2263–2275 (2024).
129. Meredith, M. et al. Polar regions. In *IPCC Special Report on the Ocean and Cryosphere in a Changing Climate* (eds Pörtner, H.-O. et al.) 203–320 (Cambridge Univ. Press, 2019).
130. Otosaka, I. N. et al. Mass balance of the Greenland and Antarctic ice sheets from 1992 to 2020. *Earth Syst. Sci. Data* **15**, 1597–1616 (2023).
131. Spence, P. et al. Rapid subsurface warming and circulation changes of Antarctic coastal waters by poleward shifting winds. *Geophys. Res. Lett.* **41**, 4601–4610 (2014).
132. Verfaillie, D. et al. The circum-Antarctic ice-shelves respond to a more positive Southern Annular Mode with regionally varied melting. *Commun. Earth Environ.* **3**, 139 (2022).
133. Pritchard, H. D. et al. Antarctic ice-sheet loss driven by basal melting of ice shelves. *Nature* **484**, 502–505 (2012).
134. Heywood, K. et al. Between the devil and the deep blue sea: the role of the Amundsen Sea continental shelf in exchanges between ocean and ice shelves. *Oceanography* **29**, 118–129 (2016).
135. Schmidtko, S., Heywood, K. J., Thompson, A. F. & Aoki, S. Multidecadal warming of Antarctic waters. *Science* **346**, 1227–1231 (2014).
136. Cook, A. J. et al. Ocean forcing of glacier retreat in the western Antarctic Peninsula. *Science* **353**, 283–286 (2016).
137. Jenkins, A. et al. Decadal ocean forcing and Antarctic ice sheet response: lessons from the Amundsen Sea. *Oceanography* **29**, 106–117 (2016).
138. Kimura, S. et al. Oceanographic controls on the variability of ice-shelf basal melting and circulation of glacial meltwater in the Amundsen Sea Embayment, Antarctica. *J. Geophys. Res. Ocean.* **122**, 10131–10155 (2017).
139. Dinniman, M. S., Klinck, J. M. & Hofmann, E. E. Sensitivity of circumpolar deep water transport and ice shelf basal melt along the West Antarctic Peninsula to changes in the winds. *J. Clim.* **25**, 4799–4816 (2012).
140. Zhang, Z. et al. Linkage of the physical environments in the northern Antarctic Peninsula region to the Southern Annular Mode and the implications for the phytoplankton production. *Prog. Oceanogr.* **188**, 102416 (2020).
141. Hazel, J. E. & Stewart, A. L. Are the near-Antarctic easterly winds weakening in response to enhancement of the Southern Annular Mode? *J. Clim.* **32**, 1895–1918 (2019).
142. Meijers, A. J. S. The Southern Ocean in the Coupled Model Intercomparison Project phase 5. *Philos. Trans. R. Soc. Math. Phys. Eng. Sci.* **372**, 20130296 (2014).
143. Downes, S. M. & Hogg, A. M. Southern Ocean circulation and eddy compensation in CMIP5 models. *J. Clim.* **26**, 7198–7220 (2013).
144. Spence, P. et al. Localized rapid warming of West Antarctic subsurface waters by remote winds. *Nat. Clim. Change* **7**, 595–603 (2017).
145. Holland, P. R., Bracegirdle, T. J., Dutrieux, P., Jenkins, A. & Steig, E. J. West Antarctic ice loss influenced by internal climate variability and anthropogenic forcing. *Nat. Geosci.* **12**, 718–724 (2019).
146. Purich, A. & England, M. H. Historical and future projected warming of Antarctic shelf bottom water in CMIP6 models. *Geophys. Res. Lett.* **48**, e2021GL092752 (2021).
147. Hosking, J. S., Orr, A., Bracegirdle, T. J. & Turner, J. Future circulation changes off West Antarctica: sensitivity of the Amundsen Sea Low to projected anthropogenic forcing. *Geophys. Res. Lett.* **43**, 367–376 (2016).
148. Neme, J., England, M. H. & McC. Hogg, A. Projected changes of surface winds over the Antarctic continental margin. *Geophys. Res. Lett.* **49**, e2022GL098820 (2022).
149. Marshall, G. J. Half-century seasonal relationships between the Southern Annular Mode and Antarctic temperatures. *Int. J. Climatol.* **27**, 373–383 (2007).
150. Thompson, D. W. J. & Solomon, S. Interpretation of recent Southern Hemisphere climate change. *Science* **296**, 895–899 (2002).
151. Marshall, G. J. & Thompson, D. W. J. The signatures of large-scale patterns of atmospheric variability in Antarctic surface temperatures. *J. Geophys. Res. Atmos.* **121**, 3276–3289 (2016).
152. Saunderson, D., Mackintosh, A. N., McCormack, F. S., Jones, R. S. & van Dalum, C. T. How does the Southern Annular Mode control surface melt in East Antarctica? *Geophys. Res. Lett.* **51**, e2023GL105475 (2024).
153. Van Den Broeke, M. R. & Van Lipzig, N. P. M. Changes in Antarctic temperature, wind and precipitation in response to the Antarctic Oscillation. *Ann. Glaciol.* **39**, 119–126 (2004).
154. Reid, K. J., Arblaster, J. M., Alexander, L. V. & Siems, S. T. Spurious trends in high latitude Southern Hemisphere precipitation observations. *Geophys. Res. Lett.* **51**, e2023GL106994 (2024).
155. Marshall, G. J., Thompson, D. W. J. & van den Broeke, M. R. The signature of Southern Hemisphere atmospheric circulation patterns in Antarctic precipitation. *Geophys. Res. Lett.* **44**, 11,580–11,589 (2017).
156. Wille, J. D. et al. Antarctic atmospheric river climatology and precipitation impacts. *J. Geophys. Res. Atmos.* **126**, e2020JD033788 (2021).
157. Hartmann, D. L. A PV view of zonal flow vacillation. *J. Atmos. Sci.* **52**, 2561–2576 (1995).
158. Turner, J. et al. The dominant role of extreme precipitation events in Antarctic snowfall variability. *Geophys. Res. Lett.* **46**, 3502–3511 (2019).
159. Previdi, M. & Polvani, L. M. Impact of the montreal protocol on Antarctic surface mass balance and implications for global sea level rise. *J. Clim.* **30**, 7247–7253 (2017).
160. Chemke, R., Previdi, M., England, M. R. & Polvani, L. M. Distinguishing the impacts of ozone and ozone-depleting substances on the recent increase in Antarctic surface mass balance. *Cryosphere* **14**, 4135–4144 (2020).
161. Medley, B. & Thomas, E. R. Increased snowfall over the Antarctic ice sheet mitigated twentieth-century sea-level rise. *Nat. Clim. Change* **9**, 34–39 (2019).
162. Dalaiden, Q., Goosse, H., Lenaerts, J. T. M., Cavitte, M. G. P. & Henderson, N. Future Antarctic snow accumulation trend is dominated by atmospheric synoptic-scale events. *Commun. Earth Environ.* **1**, 62 (2020).

163. Zhang, B., Yao, Y., Liu, L. & Yang, Y. Interannual ice mass variations over the Antarctic ice sheet from 2003 to 2017 were linked to El Niño–Southern Oscillation. *Earth Planet. Sci. Lett.* **560**, 116796 (2021).
164. Pfeffer, J., Cazenave, A. & Barnoud, A. Analysis of the interannual variability in satellite gravity solutions: detection of climate modes fingerprints in water mass displacements across continents and oceans. *Clim. Dyn.* **58**, 1065–1084 (2022).
165. Kim, B.-H., Seo, K.-W., Eom, J., Chen, J. & Wilson, C. R. Antarctic ice mass variations from 1979 to 2017 driven by anomalous precipitation accumulation. *Sci. Rep.* **10**, 20366 (2020).
166. King, M. A., Lyu, K. & Zhang, X. Climate variability a key driver of recent Antarctic ice-mass change. *Nat. Geosci.* **16**, 1128–1135 (2023).
167. Frölicher, T. L. et al. Dominance of the Southern Ocean in anthropogenic carbon and heat uptake in CMIP5 models. *J. Clim.* **28**, 862–886 (2015).
168. Landschützer, P. et al. The reinvigoration of the Southern Ocean carbon sink. *Science* **349**, 1221–1224 (2015).
169. Menviel, L. & Spence, P. Southern Ocean circulation's impact on atmospheric CO_2 concentration. *Front. Mar. Sci.* **10**, 1328534 (2024).
170. Lenton, A. & Matear, R. J. Role of the Southern Annular Mode (SAM) in Southern Ocean CO_2 uptake. *Glob. Biogeochem. Cycles* **21**, 2006GB002714 (2007).
171. Lovenduski, N. S., Gruber, N., Doney, S. C. & Lima, I. D. Enhanced CO_2 outgassing in the Southern Ocean from a positive phase of the Southern Annular Mode. *Glob. Biogeochem. Cycles* **21**, GB2026 (2007).
172. Hauck, J. et al. Seasonally different carbon flux changes in the Southern Ocean in response to the Southern Annular Mode. *Glob. Biogeochem. Cycles* **27**, 1236–1245 (2013).
173. Sallée, J.-B., Speer, K. G. & Rintoul, S. R. Zonally asymmetric response of the Southern Ocean mixed-layer depth to the Southern Annular Mode. *Nat. Geosci.* **3**, 273–279 (2010).
174. Dufour, C. O. et al. Eddy compensation and controls of the enhanced sea-to-air CO_2 flux during positive phases of the Southern Annular Mode. *Glob. Biogeochem. Cycles* **27**, 950–961 (2013).
175. Menviel, L. C. et al. Enhanced Southern Ocean CO_2 outgassing as a result of stronger and poleward shifted Southern Hemispheric westerlies. *Biogeosciences* **20**, 4413–4431 (2023).
176. Sallée, J.-B., Matear, R. J., Rintoul, S. R. & Lenton, A. Localized subduction of anthropogenic carbon dioxide in the Southern Hemisphere oceans. *Nat. Geosci.* **5**, 579–584 (2012).
177. Ito, T., Woloszyn, M. & Mazloff, M. Anthropogenic carbon dioxide transport in the Southern Ocean driven by Ekman flow. *Nature* **463**, 80–83 (2010).
178. Keppler, L. & Landschützer, P. Regional wind variability modulates the Southern Ocean carbon sink. *Sci. Rep.* **9**, 7384 (2019).
179. Swart, N. C., Gille, S. T., Fyfe, J. C. & Gillett, N. P. Recent Southern Ocean warming and freshening driven by greenhouse gas emissions and ozone depletion. *Nat. Geosci.* **11**, 836–841 (2018).
180. Cai, W. et al. Southern Ocean warming and its climatic impacts. *Sci. Bull.* **68**, 946–960 (2023).
181. Ayers, J. M. & Strutton, P. G. Nutrient variability in subAntarctic mode waters forced by the Southern Annular Mode and ENSO. *Geophys. Res. Lett.* **40**, 3419–3423 (2013).
182. de Baar, H. J. W., Buma, A., Nolting, R., Cadee, G. & Jacques, G. On iron limitation of the Southern Ocean: experimental observations in the Weddell and Scotia seas. *Mar. Ecol. Prog. Ser.* **65**, 105–122 (1990).
183. Lovenduski, N. S. & Gruber, N. Impact of the Southern Annular Mode on Southern Ocean circulation and biology. *Geophys. Res. Lett.* **32**, L11603 (2005).
184. Noh, K. M., Lim, H.-G. & Kug, J.-S. Zonally asymmetric phytoplankton response to the Southern Annular Mode in the marginal sea of the Southern Ocean. *Sci. Rep.* **11**, 10266 (2021).
185. Greaves, B. L. et al. The Southern Annular Mode (SAM) influences phytoplankton communities in the seasonal ice zone of the Southern Ocean. *Biogeosciences* **17**, 3815–3835 (2020).
186. Li, Q., England, M. H., Hogg, A. M., Rintoul, S. R. & Morrison, A. K. Abyssal ocean overturning slowdown and warming driven by Antarctic meltwater. *Nature* **615**, 841–847 (2023).
187. Revell, L. E., Robertson, F., Douglas, H., Morgenstern, O. & Frame, D. Influence of ozone forcing on 21st century Southern Hemisphere surface westerlies in CMIP6 models. *Geophys. Res. Lett.* **49**, e2022GL098252 (2022).
188. Yeager, S. G. et al. Reduced Southern Ocean warming enhances global skill and signal-to-noise in an eddy-resolving decadal prediction system. *npj Clim. Atmos. Sci.* **6**, 107 (2023).
189. Hartmann, D. L. The Antarctic ozone hole and the pattern effect on climate sensitivity. *Proc. Natl Acad. Sci. USA* **119**, e2207889119 (2022).
190. Zhang, X. et al. Evaluation of the seasonality and spatial aspects of the Southern Annular Mode in CMIP6 models. *Int. J. Climatol.* **42**, 3820–3837 (2022).
191. Udy, D. G., Vance, T. R., Kiem, A. S. & Holbrook, N. J. A synoptic bridge linking sea salt aerosol concentrations in East Antarctic snowfall to Australian rainfall. *Commun. Earth Environ.* **3**, 175 (2022).
192. Silvestri, G. E. & Vera, C. S. Antarctic oscillation signal on precipitation anomalies over southeastern South America. *Geophys. Res. Lett.* **30**, 2115 (2003).
193. Vasconcellos, F. C. & Cavalcanti, I. F. A. Extreme precipitation over Southeastern Brazil in the austral summer and relations with the Southern Hemisphere annular mode. *Atmos. Sci. Lett.* **11**, 21–26 (2010).
194. Smith, D. M. et al. Attribution of multi-annual to decadal changes in the climate system: the Large Ensemble Single Forcing Model Intercomparison Project (LESFMIP). *Front. Clim.* **4**, 955414 (2022).
195. Fiddes, S. L., Protat, A., Mallet, M. D., Alexander, S. P. & Woodhouse, M. T. Southern Ocean cloud and shortwave radiation biases in a nudged climate model simulation: does the model ever get it right? *Atmos. Chem. Phys.* **22**, 14603–14630 (2022).
196. Turner, J. & Comiso, J. Solve Antarctica's sea-ice puzzle. *Nature* **547**, 275–277 (2017).
197. Eyring, V. et al. Overview of the Coupled Model Intercomparison Project phase 6 (CMIP6) experimental design and organization. *Geosci. Model Dev.* **9**, 1937–1958 (2016).
198. Mo, K. C. Relationships between low-frequency variability in the Southern Hemisphere and sea surface temperature anomalies. *J. Clim.* **13**, 3599–3610 (2000).
199. Schmidt, G. A. et al. Climate forcing reconstructions for use in PMIP simulations of the last millennium (v1.0). *Geosci. Model Dev.* **4**, 33–45 (2011).
200. Meier, W., Fetterer, F., & Windnagel, A. *NOAA/NSIDC Climate Data Record of Passive Microwave Sea Ice Concentration, Version 4* (National Snow and Ice Data Center, 2021).
201. Hersbach, H. et al. The ERA5 global reanalysis. *Q. J. R. Meteorol. Soc.* **146**, 1999–2049 (2020).
202. Seviour, W. J. M. et al. Skillful seasonal prediction of the Southern Annular Mode and Antarctic ozone. *J. Clim.* **27**, 7462–7474 (2014).
203. Trenberth, K. E. The definition of El Niño. *Bull. Am. Meteorol. Soc.* **78**, 2771–2778 (1997).
204. Ashok, K., Behera, S. K., Rao, S. A., Weng, H. & Yamagata, T. El Niño Modoki and its possible teleconnection. *J. Geophys. Res. Oceans* https://doi.org/10.1029/2006JC003798 (2007).

Acknowledgements

The initial draft for this manuscript was written at a workshop held in Melbourne in May 2024, funded by the United States Office of Naval Research Global (N62909-23-1-2097). This work was supported by the Australian Research Council, including the Special Research Initiative for Securing Antarctica's Environmental Future (SR200100005), the Special Research Initiative Australian Centre for Excellence in Antarctic Science (SR200100008), the Centre of Excellence for Climate Extremes (CE17010023), the Centre of Excellence for Weather of the 21st Century (CE230100012), Discovery Projects DP230102994 and DP190100494, Discovery Early Career Research Award DE200100414, and Future Fellowship FT190100413, funded by the Australian Government. This project also received grant funding from the Australian Government as part of the Antarctic Science Collaboration Initiative programme (ASCI000002), the National Environmental Science Program and the Victorian Government's Water and Climate Initiative. This research was undertaken with the assistance of resources and services from the National Computational Infrastructure, which is supported by the Australian Government. The authors thank S. McCormack for the assistance preparing Fig. 7. The authors also thank C. Chung, D. Jakob and D. Jones for their comments on the paper.

Author contributions

A.P., J.M.A., M.H.E., M.J. and E.-P.L. conceived the Review. A.P. organized the writing workshop and led the overall coordination of the paper. Z.E.G. led the dynamics section, J.M.A. led the trends and projections section, and W.H. led the impacts section. G.B. prepared Figs. 1,4 and 5, M.J. prepared Fig. 2, V.G.O. prepared Fig. 3, R.R. prepared Fig. 6, and W.H. and A.P. designed Fig. 7. All authors wrote the initial manuscript, reviewed, edited and improved the paper.

Competing interests

The authors declare no competing interests.

Additional information

Peer review information *Nature Reviews Earth & Environment* thanks Deborah Verfaillie, Xiaoqiao Wang, Zhaoru Zhang and the other, anonymous, reviewer(s) for their contribution to the peer review of this work.

Publisher's note Springer Nature remains neutral with regard to jurisdictional claims in published maps and institutional affiliations.

Springer Nature or its licensor (e.g. a society or other partner) holds exclusive rights to this article under a publishing agreement with the author(s) or other rightsholder(s); author self-archiving of the accepted manuscript version of this article is solely governed by the terms of such publishing agreement and applicable law.

© Springer Nature Limited 2025

[1]School of Earth, Atmosphere and Environment, Monash University, Clayton, Kulin Nations, Victoria, Australia. [2]ARC Special Research Initiative for Securing Antarctica's Environmental Future, Clayton, Kulin Nations, Victoria, Australia. [3]ARC Centre of Excellence for Climate Extremes, Eora Nation, Sydney, New South Wales, Australia. [4]Research Bureau of Meteorology, Melbourne, Kulin Nations, Victoria, Australia. [5]Institute for Marine and Antarctic Studies, University of Tasmania, nipaluna/Hobart, Tasmania, Australia. [6]Australian Antarctic Program Partnership, nipaluna/Hobart, Tasmania, Australia. [7]Climate Change Research Centre, University of New South Wales, Eora Nation, Sydney, New South Wales, Australia. [8]ARC Australian Centre for Excellence in Antarctic Science, nipaluna/Hobart, Tasmania, Australia. [9]Research School of Earth Sciences, Australian National University, Ngunnawal and Ngambri Country, Canberra, Australian Capital Territory, Australia. [10]Centre for Marine Science and Innovation and ARC Australian Centre for Excellence in Antarctic Science, University of New South Wales, Eora Nation, Sydney, New South Wales, Australia. [11]School of Geography, Earth and Atmospheric Sciences, University of Melbourne, Parkville, Kulin Nations, Victoria, Australia. [12]ARC Centre of Excellence for the Weather of the 21st Century, nipaluna/Hobart, Tasmania, Australia. [13]CSIRO Environment, Aspendale, Kulin Nations, Victoria, Australia.